Succinate is Broadly Tissue-Permeant and Uncouples Mitochondrial Respiration from ATP Synthesis

Daniel T. Hass[1], Brian M. Robbings[1,2], Celia M. Bisbach[1], Elizabeth Giering[3], Thomas O. Mundinger[3], Martin Sadilek[4], Ian R. Sweet[2], James B. Hurley[1*]

[1]*Biochemistry Department, The University of Washington, Seattle WA 98109*
[2]*Diabetes Institute, The University of Washington, Seattle WA 98109*
[3]*Division of Endocrinology/Metabolism, Veterans Affairs Puget Sound Health Care System, Seattle, WA*
[4]*Chemistry Department, The University of Washington, Seattle WA 98109*

**Corresponding author; contact: jbhhh@uw.edu*

Abstract

Succinate is a mitochondrial metabolite well known for its ability to stimulate respiration through succinate dehydrogenase. Data from multiple studies have implied that succinate localized to mitochondria and does not cross tissue boundaries. We tested this hypothesis by infusing ^{13}C-labeled succinate into the bloodstream of awake, moving C57BL6/J mice through a jugular catheter. Following the infusion we probed intermediates of glycolytic and Krebs cycle metabolism to determine how different tissues utilize succinate. We found that retina and eyecup metabolism appeared unique in their handling of succinate. The retina appeared to be the least permeant to succinate, and succinate that was taken up was not well integrated into the Krebs cycle and was rather directed to become glycolytic intermediates. In the eyecup, ^{13}C originating from succinate populated Krebs cycle intermediates particularly well. We also found that *ex vivo*, succinate stimulates mitochondrial uncoupling in eyecup tissue, which may be particularly relevant in the biology of the eye, as retina tissue secretes succinate.

Introduction

Succinate is a key intermediate in the Krebs cycle and electron transport chain (ETC). Conversion of succinate to fumarate by succinate dehydrogenase (SDH) provides an input of electrons that reduce coenzyme Q_{10} (QH_2) in the ETC. The flow of electrons QH_2 to O_2 via ETC complexes is coupled to proton (H^+) translocation from the mitochondrial matrix to the intermembrane space. Constitutive H^+ translocation forms a proton motive force ($\Delta\rho$) across the inner mitochondrial membrane. $\Delta\rho$ powers ATP synthesis, and transport of P_i, pyruvate, glutamate, and adenine nucleotides into the mitochondrial matrix (Gutiérrez-Aguilar & Baines, 2013). By donating electrons to the ETC, succinate can help to form $\Delta\rho$.

The current literature suggests that exogenous succinate is not imported into most cells (Ehinger et al., 2016), despite widespread expression of monocarboxylate and dicarboxylate transporters capable of carrying succinate across the plasma membrane (Andrienko et al., 2017; Nakai et al., 2006; Pajor, 2014; Prag et al., 2020). Succinate is believed to be produced primarily in muscle (Hochachka & Dressendorfer, 1976), pancreas (Jang et al., 2019), and possibly by gut microbiota (Serena et al., 2018). It is thought to be consumed primarily in brown adipose tissue to fuel thermogenesis (Mills et al., 2018), though extracellular succinate also drastically increases respiration in *ex vivo* eyecup tissue (consisting of sclera, choroid, and retinal pigment epithelium) (Bisbach et al., 2020). This suggests the presence of additional cell types capable of oxidizing exogenous succinate, which may or may not be limited to eyecup tissue.

We investigated succinate metabolism in a panel of tissues *ex vivo* to determine which of them catabolize succinate, and *in vivo* to determine how that succinate is metabolized. We found that most

tissues exhibit a robust ability to oxidize succinate, with unique destinations for succinate carbons in retina and eyecup tissue. We also found that succinate uncouples mitochondrial respiration from ATP synthesis. This uncoupling is not linked with oxidative stress, adenine nucleotide transporter activity, or mitochondrial permeability transition pore complex activity, and we suggest that extracellular succinate is instead capable of directly uncoupling mitochondria through mitochondrial membrane potential-dependent increases in H^+-leak.

Materials and Methods

Ethical Approval

This study was carried out in accordance with the National Research Council's Guide for the Care and Use of Laboratory Animals (*8th ed*). All protocols were approved by the Institutional Animal Care and Use Committees at the University of Washington and the VA Puget Sound Hospital.

Animals

In all experiments, we used 2-5 month-old wild-type C57BL6/J mice. These mice were housed at an ambient temperature of 25°C, with a 12-hour light cycle and *ad libitum* access to water and normal rodent chow.

Small animal surgeries

The procedure for chronic jugular vein and carotid artery catheterization was performed as previously described (Ayala et al., 2011) by the Cell Function and Analysis Core of the University of Washington's Diabetes Research Center. Briefly, following induction and maintenance under systemic inhaled anesthesia (isoflurane 1.5-2% in 1L/min), mice were administered with 4 mg/kg ketoprofen to reduce post-surgical swelling and provide analgesia. For intravenous infusions, jugular veins for were isolated through a lateral incision to the trachea, and a silastic catheter was introduced into the vein, anchored to surrounding tissue, tunneled subcutaneously to the nape of the neck and connected to a vascular access port. A subset of mice received a contralateral carotid artery cannulation for blood sampling. The catheters were filled with heparinized saline, the skin incisions were sutured, and the mice recovered for 1 week before conscious infusion studies.

In vivo infusions

Jugular vein infusion studies were performed on freely moving, chronically cannulated. This system allows us to avoid the potential confounding effects of acute surgical stress (Walters et al., 2016) or anesthesia (Windeløv et al., 2016) on succinate uptake or metabolism. We infused 100 mg/kg U-^{13}C-succinate (Cambridge Isotopes, CLM-1571) through jugular catheters over a period of approximately 20 seconds and euthanized mice by awake cervical dislocation 1, 2, 3, 5, or 10 minutes following the infusion. When mice possessed both carotid artery and jugular vein catheters, we took two 10 µL baseline blood samples per mouse then infused 100 mg/kg U-^{13}C-succinate through the jugular catheter. We sampled 10 µL of blood 0.5, 1, 2, 3, 4, 5, 7.5, and 10 minutes following the infusion, then euthanized mice. Following euthanasia we quickly dissected retinas and eyecups (a complex of the retinal pigment epithelium, sclera, and choroid vasculature) from the eye. For the 5 minutes post-infusion time point, we also dissected liver, lung, cerebellum, interscapular white adipose tissue, and interscapular brown adipose tissue. Dissected tissues were snap frozen in liquid N_2. All mice were euthanized between 10 AM and 1 PM to minimize circadian effects on metabolic function.

Ex vivo metabolic flux

In all ex vivo labeling experiments, we quickly euthanized mice by awake cervical dislocation, dissected the indicated tissues in Hank's Buffered Salt Solution (HBSS; GIBCO, Cat#: 14025-076), and incubated them in pH 7.4 Krebs-Ringer bicarbonate (KRB) buffer (98.5 mM NaCl, 4.9 mM KCl,

1.2 mM KH_2PO_4 1.2 mM $MgSO_4$-$7H_2O$, 20 mM HEPES, 2.6 mM $CaCl_2$-$2H_2O$, 25.9 mM $NaHCO_3$) supplemented with 5 mM glucose and [U-^{13}C]-succinic acid (Cambridge isotope CLM-1571-0.1; concentrations indicated in figures). This buffer was pre-equilibrated at 37°C, 21% O_2, and 5% CO_2 prior to incubations. Following incubations, tissue was flash frozen in liquid nitrogen.

Metabolite Extraction

Metabolites were extracted using 80% MeOH, 20% H_2O supplemented with 10 µM methylsuccinate (Sigma, M81209) as an internal standard to adjust for any metabolite loss during the extraction and derivatization procedures. The extraction buffer was equilibrated on dry ice, and 150 µL was added to each sample. Tissues were then disrupted by sonication and incubated on dry ice for 45 minutes to precipitate protein. Proteins were pelleted at 17,000 x g for 30 minutes at 4°C. The supernatant containing metabolites was lyophilized at room-temperature until dry and stored at -80°C until derivatization. The pellet containing protein was resuspended by sonication in RIPA buffer (150 mM NaCl, 1.0% Triton X-100, 0.5% sodium deoxycholate, 0.1% SDS, 50 mM Tris, pH 8.0) and the amount of protein was determined by a BCA assay (ThermoFischer, 23225).

Metabolite Derivatization

Lyophilized samples were first derivatized in 10 µL of 20 mg/mL methoxyamine HCl (Sigma, Cat#: 226904) dissolved in pyridine (Sigma, Cat#: 270970) at 37°C for 90 minutes, and subsequently with 10 µL tert-butyldimethylsilyl-N-methyltrifluoroacetamide (Sigma, Cat#: 394882) at 70°C for 60 minutes.

Gas Chromatography-Mass Spectrometry

Metabolites were analyzed on an Agilent 7890/5975C GC-MS using selected-ion monitoring methods described extensively in previous work (Du et al., 2015). Peaks were integrated in MSD ChemStation (Agilent), and correction for natural isotope abundance was performed using the software IsoCor (Millard et al., 2019). Corrected metabolite signals were converted to molar amounts by comparing metabolite peak abundances in samples with those in a 'standard mix' containing known quantities of metabolites we routinely measure. Multiple concentrations of this mix were extracted, derivatized, and run alongside samples in each experiment. These known metabolite concentrations were used to generate a standard curve which allowed for metabolite quantification. Metabolite abundance was normalized to tissue protein concentration, and following this, paired tissues such as retinas and eyecups from the same mouse were treated as technical replicates and averaged.

Ex vivo oxygen consumption

Following euthanasia, mouse tissues were dissected and cut into small segments in Hank's buffered salt solution. These tissues were incubated in Krebs-Ringer bicarbonate buffer (KRB) supplemented with 5 mM glucose and pre-equilibrated at 37°C and 5% CO_2. We determined OCR using a custom-built perifusion flow-culture system (Sweet et al., 2002; Neal et al., 2015). Tissues were perifused in chambers between Cytopore beads (Amersham Biosciences, Piscatawy, NJ) and porous frits. With KRB supplemented with 5 mM glucose, 1x Antibiotic-Antimycotic (Gibco), and 0.1 g/ 100 mL fatty acid-free bovine serum albumin. An artificial lung oxygenated supplemented KRB with a mixture of 21% O_2, 5% CO_2, and 74% N_2, and this media was passed through a bubble trap before moving through the chambers containing mouse tissues. Outflow media came into contact with a glass wall coated with a thin layer of oxygen sensitive polymerized Pt(II) Meso-tetra(pentafluorophenyl)porphine dye (Frontier Scientific, Logan, UT) painted on the inner glass wall of the chamber. Following a 405 nm light pulse, the dye-coated glass emits a phosphorescent signal detected at 650 nm. The decay lifetime is dependent on oxygen tension. The flow rate of KRB along with the quantitative relationship between dye phosphorescent decay and oxygen concentration were used to determine tissue OCR. All OCR measurements were obtained under control conditions (baseline, 5 mM glucose), one or

more experimental conditions, and a 'zeroed' condition wherein 3 mM potassium cyanide (KCN) was used to directly inhibit complex IV and thus subtract the effect of residual non-mitochondrial oxygen consumption from our measurements.

Western Blot

Protein was extracted by sonication in RIPA buffer supplemented with a protease and phosphatase inhibitor cocktails (ThermoFisher, Cat#: 78442). SDS sample buffer was added and samples were run on 13% polyacrylamide gels. After running, gels were transferred onto PVDF membranes (Millipore, IPFL00010) and rinsed with PBS. Primary antibody (anti-Total Oxphos, 1:1000 dilution, RRID: AB_2629281, Lot# P3338) was diluted in blocking buffer (LI-COR, 927–40,000) and incubated overnight on blots at 4°C. Membranes were washed twice with PBS containing 0.1% Tween-20 and once with PBS, then incubated with secondary antibody (IRDye 800CW goat anti-mouse IgG (H + L) (LI- COR Biosciences, 925-32210, RRID: AB_2687825) at 1:5000 in blocking buffer for 1 h at RT and washed again before imaging. Membranes were imaged and bands were quantified using the LI-COR Odyssey CLx Imaging System (RRID:SCR_014579).

Statistical Analysis [Incomplete]

We performed all statistical data analysis using Prism Version 8 (GraphPad Software). We fit curves of [m+4 succinate] over time with a one-phase exponential decay equation (after time = 0 minutes) to determine the half-life of infused m+4 succinate in blood. To fit curves of oxygen consumption as a function of [succinate], for each sample we averaged steady-state oxygen consumption over >5 minutes at the end of a given treatment. These averaged values were considered to be the OCR at each given [succinate] for each sample. We fit the curve to an allosteric sigmoidal shape in order to obtain approximations of V_{max}, $K_{1/2}$, and Hill's coefficient (h).

Results

Extracellular Succinate Promotes O_2 Flux Ex Vivo

In the conventional Krebs cycle, succinate dehydrogenase oxidizes succinate to fumarate. The hydrogen atoms removed from succinate reduce coenzyme Q_{10}. Electrons from reduced coenzyme Q_{10} (QH_2) are transferred to cytochrome C then to O_2, forming H_2O (**Figure 1A**). Oxidation of succinate by this pathway stimulates O_2 consumption. We measured mitochondrial O_2 consumption rate (OCR) by quantifying KCN-sensitive changes in OCR. KCN is an inhibitor of cytochrome oxidase (complex IV) the mitochondrial enzyme that converts O_2 to H_2O. We determined the OCR as a function of extracellular succinate concentration in modified Krebs-Ringer Bicarbonate (KRB) buffer supplemented with 5 mM glucose (**Figure 1B-H**). Examples of the data obtained in typical experiments are pictured in **Figure 1B**. In ex vivo liver, cerebellum, BAT, kidney, eyecup (a complex of retinal pigment epithelium, choroid, and sclera), and retina tissue, increasing succinate concentrations (30 µM, 100 µM, 300 µM, 1 mM, 3 mM, 10 mM, 30 mM, and 100 mM) stimulated OCR. To remove the contribution of glucose to mitochondrial respiration, we subtracted the basal respiration (OCR with 5 mM glucose alone) from succinate-stimulated OCR to obtain pseudo-kinetic curves of OCR as a function of succinate concentration (**Figure 1C-H**). We fit these curves with an allosteric sigmoidal function, and found $K_{1/2}$ values ranging from 0.9-2.77 mM (**Table 1**) for all tissues except the retina, which had a $K_{1/2}$ of 11.14 mM. This unusually high $K_{1/2}$ estimate is a lower limit generated by curve fitting because the retinal OCR did not reach saturation at the succinate concentrations used in our experiments. The unusual concentration-dependance of succinate-stimulated OCR in the retina suggests that mitochondrial metabolism of exogenous succinate is substantially different between the retina and other tissues. Succinate can stimulate the SUCNR1, a G-protein coupled receptor that stimulates a multitude of metabolic effects (Prag et al., 2020; Wang et

al., 2020). However, the SUCNR1 agonist, cis-epoxysuccinate (500 µM), did not stimulate O_2 consumption (**Figure S1**).

Infused Succinate is Metabolized In Vivo

Ex vivo experiments are a powerful means by which to approximate the physiology of succinate *in vivo*, but the tissue isolation process may impact cell integrity and thus plasma membrane or mitochondrial succinate permeability. We tested whether succinate import into cells occurs *in vivo* by infusing male and female C57BL6/J mice with a 100 mg/kg bolus of uniformly labeled (U)-^{13}C succinate dissolved in sterile saline (pH 7.4). We first infused mice with dual carotid artery and jugular vein catheters. We withdrew two 10 µL baseline whole blood samples through the carotid catheter, then infused labeled succinate through the jugular catheter. We sampled 10 µL of blood at 0.5, 1, 2, 3, 4, 5, 7.5, and 10 minutes following the infusion and used gas chromatography–mass spectrometry (GC-MS) to measure the accumulation of ^{13}C on metabolites in glycolysis and the Krebs cycle (**Table 2**). Total blood U-^{13}C-succinate levels(noted in figures as m+4 because it contains four ^{13}C-labeled carbon atoms) spiked immediately following infusion and rapidly declined throughout the 10-minute process (**Figure 2A**). A single exponential fit of m+4 succinate over time shows that infused succinate reached a half maximal concentration at 0.88 (95% CI: 0.04 - 3.32) minutes post-infusion, which is more rapid than consumption of infused glucose (Parilla et al., 2018). The dominant isotopologue in blood was m+4, showing that for at least 10 minutes following the bolus infusion, tissues have access to a pool of almost fully labeled succinate (**Figure 2B**). A molecule in blood spectrally overlaps with m+4 succinate. It can interferes with a completely accurate estimation of succinate isotopologue distribution. However, this signal contaminant contributes ~3.7% of the m+4 succinate signal 10 minutes following infusion, so it does not cause major errors in the isotopic correction algorithm in post-infusion blood samples. Following the bolus infusion, m+4 labeling also appears in circulating fumarate and malate pools, and is cleared by the time m+4 succinate is (**Figure S2**).

Five minutes after infusion, m+4 succinate labels the retina, cerebellum, eyecup, liver, lung, interscapular brown adipose tissue (BAT), and interscapular white adipose tissue (WAT) (**Figure 2C**). We estimated succinate turnover in these tissues from the fraction of succinate that is m+4. Fractional labeling was highest in blood, eyecup, lung, BAT, and WAT, with relatively minimal fractional labeling of succinate in retina, cerebellum, or liver (**Figure 2D**). Fractional labeling depends on overall succinate pool size and a low fractional labeling does not necessarily mean a tissue is not metabolizing succinate. We also estimated succinate catabolism in this tissue panel by summing the molar abundance of ^{13}C (originating from U-^{13}C-succinate) on all metabolites that we routinely measure. We normalized this quantity to the molar abundance of ^{12}C in the same sample (**Figure 2E**). A substantial portion of metabolites in eyecup, brown adipose tissue, and blood were labeled with ^{13}C. A list of these metabolites is available in **Table S2,** succinate itself was excluded from this analysis of downstream meatabolism. Retina accumulated less succinate than other tissues, whereas succinate was enriched in lung and eyecup (**Figure 2C**-**D**), suggesting a relatively small succinate pool with high flux. On the other hand, tissues which accumulated similar amounts of intermediates downstream from succinate (cerebellum, liver, BAT, WAT) had lower overall replacement of the labeled succinate fraction, which implies a larger and perhaps more stationary succinate pool.

^{13}C from succinate labeled the downstream intermediate fumarate, malate, aspartate, citrate, and pyruvate in all tissues to varying degrees. Enrichment of ^{13}C-label on these metabolites is correlated with the amount of m+4 succinate present in the tissue (**Figure S3**). To compare how succinate is used among different tissue types, we normalized the abundance of these labeled metabolites to m+4 succinate. **Figure 2F** shows the isotopologues expected to appear in tissues following conventional Krebs cycle-mediated succinate catabolism. 5-minutes post-infusion we find these labeled

metabolites do accumulate, with relatively low labeling of downstream Krebs cycle intermediates in blood compared to within tissues (**Figure 2G-K**). In this panel, m+4 label from succinate accumulates as fumarate to the greatest extent in eyecups, implying that succinate oxidation may be faster in eyecup tissue than others (**Figure 2G**). Additionally, normalized to m+4 succinate, we found a roughly equivalent proportion of m+4 fumarate in the retina as many other tissues, suggesting that the poor responsiveness of the retina to succinate observed *ex vivo* occurs at the level of succinate import rather than oxidation to fumarate. Higher m+4 fumarate in eyecups also leads to more labeling in downstream intermediates such as malate (**Figure 2H**), citrate (**Figure 2I**), and aspartate (**Figure 2J**). These data suggest that SDH is twice as active in eyecups than in other tissues. We asked if the tissue differences are related to the abundance of mitochondrial content across different tissues. We measured the relative abundances of complex I, II, III, IV and V (ATP synthase) component proteins and found that eyecup SDHB levels are equal to or lower than most other tissues in the panel. This suggests that m+4 fumarate labeling is not directly linked to expression of SDHB (**Figure S4**).

Eyecups metabolize succinate similarly to other tissues, but to a greater extent per molecule of succinate. Unexpectedly, retina and no other tissue incorporates ^{13}C from m+4 succinate into m+3 pyruvate (**Figure 2K**). This suggested decarboxylation of either malate or oxaloacetate made from succinate. Since succinate catabolism in the retina and eyecup are so distinct and because these tissues are adjacent in the eye we investigated the relationship between retina and eyecup succinate metabolism in in vivo. We followed ^{13}C flux in these tissues 1, 2, 3, 5, and 12 minutes following infusion of 100 mg/kg U-^{13}C succinate.

Succinate Infusion Reveals Metabolic Specialization in the Retina and Eyecup

Initially, m+0 and m+4 succinate are the principal isotopologues in the retina and RPE following infusion. The decay of m+4 succinate following the bolus infusion represents entry of carbons from succinate into intracellular metabolic pathways. In the 12 minutes post-infusion, the eyecups metabolize ~40% of their m+4 succinate pool (**Figure 3A**), whereas retinas metabolize only ~5% of their pool (**Figure 3B**). As a consequence of higher m+4 succinate turnover in eyecups, downstream m+4 or m+3 isotopologues of malate (**Figure 3D**), aspartate (**Figure 3G**), citrate (**Figure 3J**), α-ketoglutarate (**Figure 3M**), isocitrate (**Figure S5A**), and glutamate **(Figure S5D)** accumulate to a greater extent in eyecup than retina, showing that the conventional Krebs cycle is highly active in this tissue. Lower retina succinate import and label turnover yielded lower % labeling patterns in downstream metabolic intermediates such as malate and citrate (**Figure 3E,K**).

M+0 and m+4 succinate are the principal isotopologues in the retina and eyecup following infusion, and decay following the bolus infusion as succinate carbons flow into different metabolic pathways. This decay suggests that in the 11 minutes between 1 and 12 minutes post-infusion, ~40% of the eyecup m+4 succinate pool is turned over (**Figure 3A**), whereas only ~5% of the pool is turned over in retinas (**Figure 3B**). As a consequence of higher m+4 succinate turnover in eyecups, downstream m+4 or m+3 isotopologues of malate (**Figure 3D**), aspartate (**Figure 3G**), citrate (**Figure 3J**), α-ketoglutarate (**Figure 3M**), isocitrate (**Figure S5A**), and glutamate **(Figure S5D)** accumulate more rapidly in eyecup than retina, showing that the conventional Krebs cycle is highly active in this tissue. Lower retina ^{13}C-succinate import limits label turnover yielded lower % labeling patterns in downstream metabolic intermediates such as malate and citrate (**Figure 3E,K**), though poor labeling of Krebs cycle intermediates may also be influenced by alternate metabolic pathways.

The absence of m+4 labeled aspartate and citrate, representing Krebs cycle intermediates downstream of succinate and malate suggests that either (**a**) carbons from malate in the retina are not oxidized to oxaloacetate, (**b**) that oxaloacetate is diverted away from reactions that form citrate or

aspartate, or (**c**) oxaloacetate does indeed become citrate, but the citrate pool is very large in comparison to the malate pool and dilutes the m+4 label. Analysis of pool sizes suggested that the retina citrate pool is not larger than the malate pool, so we investigated alternate metabolic pathways for malate carbons (**Figure 3**). We noticed that both in the retina and eyecup there was a steady accumulation of ^{13}C as m+3 pyruvate, phosphoenolpyruvate (PEP), and 3-phosphoglycerate (3PG) (**Figure 4A-H**). Accumulation of ^{13}C on these intermediates suggests gluconeogenic activity in both the retina and eyecup, most likely due to activity of the enzyme phosphoenolpyruvate carboxykinase (*PEPCK),* which catalyzes decarboxylation of oxaloacetate (m+4 labeled if its carbons originated as infused succinate) to m+3 phosphoenolpyruvate and m+1 CO_2. The PEP can then become m+3 3PG through the reversible steps of glycolysis, or m+3 pyruvate through activity of pyruvate kinase. M+3 3PG labeling in both tissues was unexpected, though because the eyecup far exceeds retina tissue in % succinate labeling yet generates a lower % 3PG, we believe gluconeogenic activity is far greater in retina tissue. This reaction scheme (**Figure 4I**) requires that m+4 oxaloacetate be formed before becoming m+3 PEP, and our data thus support possibility (b), though they do not rule out the potential impact of malic enzyme activity, which can form m+3 pyruvate from m+4 malate. A comparison of m+3 PEP labeling / m+4 succinate labeling in our tissue panel shows that retina, eyecup, and cerebellum are the main tissues forming m+3 PEP from succinate, while liver (a tissue known for high PEPCK expression) did not accumulate any detectable m+3 PEP. This implies that the liver is not performing gluconeogenesis that utilizes succinate as a substrate in our experiments (**Figure 4J**).

In the eyecup, m+2 labeling of metabolic intermediates from m+4 succinate is likely a consequence of conventional Krebs cycle activity, which due to isocitrate and α-ketoglutarate dehydrogenase activities removes two ^{13}Cs from the succinate backbone as $^{13}CO_2$. However, these reactions are unlikely to be the main source of m+2 labeling of Krebs cycle intermediates in the retina, because citrate pool is poorly m+4 labeled (**Figure 3K**), meaning that retina utilizes an unlabeled pool of oxaloacetate to form citrate. M+2 labeling on retina citrate is likely related to PEPCK activity. When the retina makes m+3 PEP from oxaloacetate, m+3 PEP can form m+3 pyruvate (**Figure 2K, 4B**), and pyruvate dehydrogenase (PDH) can utilize m+3 pyruvate to make m+2 labeled acetyl-CoA and m+1 CO_2 (**Figure XYZ**). That means that retina m+2 citrate is likely to made by the condensation of m+2 acetyl-CoA and unlabeled oxaloacetate.

M+3 PEP formation from PEPCK requires an m+4 oxaloacetate, and yet if there is m+4 oxaloacetate available to make m+3 PEP, that m+4 oxaloacetate should also be available to make m+4 citrate. Yet we do not see substantial accumulation of m+4 citrate, suggesting that within the retina, production of m+3 PEP (from labeled oxaloacetate) and m+2 citrate (from unlabeled oxaloacetate) occur in different metabolic compartments, with the unlabeled oxaloacetate most likely coming from a cell type that does not take up external m+4 succinate. This model may explain the lack of m+6 citrate (**Figure 3K**), as m+2 acetyl-CoA is formed in a compartment different than the one where m+4 oxaloacetate is formed. The m+2 citrate goes on to make m+2 α-ketoglutarate (**Figure 3N**), and m+2 malate (**Figure 3E**). Our metabolic flux data represents the summed activities of multiple retina cell types, and while our data does not reveal the identity of the particular cell which takes up succinate and uses it to form PEP, it does distinguish that activity from a separate cell which uses PEP-derived pyruvate to make citrate. These data reveal metabolic communication between different cell types, likely at the level of pyruvate import and export, as there are numerous transporters able to shuttle labeled pyruvate between cells.

The presence of gluconeogenesis in the eye can explain m+1 labeling on α-ketoglutarate, isocitrate, citrate, and malate (**Figure 3**). Decarboxylation of m+4 oxaloacetate or m+3 pyruvate by PEPCK or PDH generates m+1 CO_2, and any reaction in which carboxylation may occur can transfer this m+1

CO_2 to generate an m+1 labeled metabolite. There are two main carboxylation reactions known to interact with the Krebs cycle: (1) pyruvate carboxylation to oxaloacetate, and (2) reductive carboxylation of α-ketoglutarate. Both retinal α-ketoglutarate and isocitrate are m+1 labeled to a similar extent, suggesting that the isocitrate dehydrogenase reaction does not proceed in the reductive direction. Rather, pyruvate carboxylation is the more likely cause of m+1 labeling on Krebs cycle intermediates in the retina.

We attempted to confirm this gluconeogenic activity in *ex vivo* retina and eyecups incubated in 5 mM glucose + 50 μM U-^{13}C succinate for 0, 0.5, 1, 2, and 5 minutes, yet in both tissues we were unable to find substantial ^{13}C labeling on 3-PG, suggesting that whatever factors enable gluconeogenesis *in vivo* are not recapitulated in our *ex vivo* culture system (**Figure S6**).

Succinate Stimulates Mitochondrial Uncoupling in Eyecup Tissue

Eyecup succinate catabolism reveals rapid Krebs cycle (**Figure 2**) and electron transport chain (**Figure 1**) flux which matches that of many other tissues, per unit mass. The extent to which increasing concentrations of succinate stimulates mitochondrial O_2 flux (**Figure 1**) is surprising, as the capacity of tissues to oxidize mitochondrial substrates is generally thought to be limited by the mitochondrial proton motive force (Δρ). Excess substrate increases Δρ, leading to autoregulation of mitochondrial substrate oxidation. We validated this phenomenon using the conventional mitochondrial substrate pair pyruvate/malate. By increasing the concentration of these substrates and measuring eyecup OCR, we showed that these NADH-linked substrates is limited and was maximal at ~3 mM pyruvate + 3 mM malate (**Figure 5A**).

Succinate oxidation also increases OCR, but succinate oxidation is self-limiting at far higher substrate concentrations (~30 mM, **Figure 1**). However, succinate oxidation and NADH oxidation result in different levels of mitochondrial H^+ flux and thus Δρ per O_2 molecule is diminished. We converted substrate-dependent OCR (**Figure 5A**) into estimates of H^+ flux, assuming (1) all OCR above the 5 mM glucose 'baseline' is from oxidation of the supplied substrate, and (2) that each O_2 molecule consumed using NADH linked substrates catalyzed translocation of 10 H^+ while succinate-dependent OCR translocated to an H^+/O_2 ratio of 6 (**Figure 5B**). Concentration response curves from these two substrates show overlapping H^+ translocation rates at substrate concentrations of 300 μM and lower, but substrate-dependent deviations in H+ flux at [substrate] ≥ 1 mM. This mismatch in H^+ flux across complexes I-IV between substrates suggests that exogenous succinate produces a H^+ leak current across the inner mitochondrial membrane that is compensated for by additional substrate oxidation (and thus additional movement of H^+). We determined whether succinate produces H^+ leak by exposing eyecup tissue to either 5 mM succinate or 5 mM pyruvate/malate in the presence of the ATP synthase inhibitor oligomycin. Oligomycin inhibits O_2 consumption by preventing dissipation of Δρ by the ATP synthase. O_2 consumption in the presence of oligomycin represents substrate oxidation that is not inhibited by Δρ (because a H^+ leak conductance is able to take the place of H^+ conductance through ATP synthase). 5 mM succinate substantially enhanced OCR in the presence of oligomycin, while 5mM pyruvate/malate is far less effective. Leak respiration occurs at high concentrations of either metabolite, but to a gfar greater extent with succinate (**Figure 5C**).

We determined the extent to which succinate stimulates oligomycin-insensitive OCR by titrating succinate in the presence of oligomycin (**Figure 5D**). Increases in leak respiration occur at concentrations ≥ 300 μM succinate. Multiple mechanisms may drive succinate dependent H^+ leak, including (a) reactive oxygen species-induced activation of an uncoupling protein [cite], (b) activation

of H^+ leak through the adenine nucleotide translocase (ANT) [cite], (c) activation of the mitochondrial permeability transition pore complex (mPTP) [cite]. We stimulated succinate dependent H^+ leak by exposing eyecup tissue to 5 mM glucose, 10 µM oligomycin, and 5 mM succinate, and attempted to prevent succinate-stimulted leak respiration in (a)-(c) using inhibitors of oxidative stress (50 µM mitoTempo, 10 mM N-acetylcysteine; **Figure 5E**), the ANT (30 µM carboxyatractyloside; **Figure 5F**), or the mPTP complex (2 µM cyclosporine A; **Figure 5G**). None of these compounds suppressed succinate-dependent leak respiration. We also tested whether succinate-dependent leak respiration occurs due to reverse complex I activity, which could oxidize coenzyme Q_{10}, reduce NAD^+, and transport H^+ from the mitochondrial intermembrane space to the matrix. The complex I Q-site inhibitor rotenone partially suppressed leak respiration (**Figure 5H**). We initially considered this to be a consequence of inhibiting complex I reversal fueled by succinate-dependent reduction of the coenzyme Q_{10} pool. However, the effect of rotenone also could be explained by cutting off the supply of electrons from NADH that partially contributes to OCR. Glucose from the perifusion medium fuels cytosolic NADH production via glycolysis and mitochondrial NADH through pyruvate oxidation. We evaluated the contribution of glucose to OCR by removing it from the medium. If succinate causes complex I to operate in reverse, removing glucose would either not alter H^+ leak or increase it, and rotenone would still inhibit succinate-stimulated, oligomycin-insensitive OCR. Alternatively, if complex I operates in the forward mode, removing glucose removal would partially decrease OCR and prevent rotenone from affecting OCR. We found that glucose removal itself partially suppressed OCR and prevented rotenone from affecting OCR (**Figure 5I**). That indicates that the effect of succinate on H^+ leak is not caused by reversal of proton pumping through complex I.

Discussion

Succinate is a metabolite well characterized for its capability to stimulate O_2 consumption in isolated mitochondria [cite]. However, the ability of succinate to cross the plasma membrane and induce a physiological effect is debated. We show that diverse tissues can import and oxidize succinate (**Figure 1-2**). Succinate catabolism has tissue-specific metabolic effects, and can feed both conventional Krebs cycle activity and gluconeogenesis in distinct tissues (**Figure 3-4**). By acting in the Krebs cycle, succinate fuels mitochondrial O_2 consumption, and this occurs over a large range of succinate concentrations, with concentrations as high as 1 mM fueling not only conventional Krebs cycle activity, but also by allowing Krebs cycle and electron transport to continue without inhibition from feedback caused by buildup of the proton gradient (**Figure 5**).

Our *ex vivo* data shows a dynamic responsiveness of different tissues to extracellular succinate (**Figure 1**). Although succinate-dependent SUCNR1 activity is responsible for multiple effects in vivo, a potent agonist (Geubelle et al., 2017) did not alter OCR, suggesting that OCR depends primarily on the reducing power of succinate (**Figure S1**). The response to succinate is concentration-dependent, with a half-maximal effect on OCR between 0.9 and 2.7 mM in all tissues except retina (**Table 1**), wherein OCR depended only weakly on succinate (**Figure 1H**). Along with our in vivo flux data, this suggests a barrier to retinal succinate import. This unique behavior of the retina is consistent with our previous finding that retina tissue normally synthesizes and exports succinate (Bisbach et al., 2020). Exported succinate may act as a concentration gradient that opposes succinate import.

Succinate-stimulated OCR by non-retina tissues in our experiment are consistent similar findings in *ex vivo* dog heart and rabbit kidney tissue, where. In these tissues succinate also stimulates OCR (Furchgott & Shorr, 1948). However our findings are not consistent with the more frequently cited sentiment that succinate does not alter OCR in most cultured cells (Ehinger et al., 2016; MacDonald et al., 1989; Mills et al., 2018). Studies reporting succinate inaccessibility were mainly performed on cultured cells, and long-term cell culture may alter the expression of metabolite transporters (Hanu et

al., 2000). The transporters for succinate have not been fully characterized, and in addition to plasma membrane dicarboxylate transporters (Kaufhold et al., 2011), MCT1 can also export succinate (Prag et al., 2020; Reddy et al., 2020). This may apply to other MCTs as well. Therefore we can only explain the discrepancy in plasma membrane succinate permeability after we determine the expression patterns and transport activities of mono- and di-carboxylate transporters in cultured cells and animal tissue.

Our kinetic analysis (**Table 1**) reflects a combination of succinate transport across the plasma membrane, succinate transport into the mitochondrial matrix, oxidation by succinate dehydrogenase (SDH), and electron transport to O_2. One or more of these could be rate-limiting. $K_{1/2}$ simply conveys the dynamic range over which different tissues respond to succinate. While all tissues we tested take up succinate, liver, BAT, and kidney tissue are more sensitive to it than cerebellum, eyecup, and retina. This may be of less concern for retina (which produces succinate) and eyecup (which likely receives retina-produced succinate). The V_{max} (obtained at 30-100 mM succinate) may represent a capacity for mitochondria to oxidize succinate, yet because circulating [succinate] only exceeds 300 µM under extreme circumstances such as hypoxia (Hochachka et al., 1975), it is less likely to represent an OCR that occurs naturally.

Because there are caveats with ex vivo experiments, we probed succinate physiology *in vivo*. We infused a bolus of U-^{13}C-succinate into freely moving catheterized mice (**Figure 2-4)**. This approach complements our *ex vivo* OCR and flux data by probing succinate intake into cells in a physiological context. Metrics of succinate pool turnover (**Figure 2D**) and oxidation (**Figure 2E**) show that succinate is metabolized to the greatest extent in eyecup, lung, and BAT. RPE cells have a very high degree of vascular access relative to their abundance, and simple access to succinate may explain why they oxidize it so well. The ^{13}C-labeling approach metrics may even underestimate succinate oxidation in eyecup, as RPE cells may also receive an unlabeled succinate supply produced by the retina (Bisbach et al., 2020). Lung tissue also has high vascular access that may explain why m+4 succinate populates the lung succinate pool so quickly. In BAT other mechanisms may contribute to rapid succinate utilization. For example, basal uncoupling could accelerate Krebs cycle activity so that succinate is oxidized quickly to fuel thermogenesis (Mills et al., 2018).

Retina and eyecup tissue are specialized in how they utilize succinate carbons (**Figure 2G-K**). Label from ^{13}C-succinate (**Figure 2**) accumulated in intermediates from both the Krebs cycle and glycolysis, suggesting that a portion of succinate is siphoned off from the Krebs cycle to make, pyruvate, PEP and 3-PG. The portion of ^{13}C that originated as succinate and entered glycolysis is more substantial in the retina than the eyecup (**Figure 4**), suggesting that gluconeogenesis may occur in both tissue but may govern retina metabolism to a greater extent.

Several Krebs cycle intermediates in both tissues were found labeled with one ^{13}C. Pyruvate carboxylase in gluconeogenic tissue carboxylates pyruvate to form oxaloacetate. $^{13}CO_2$ is a product of both gluconeogenic and Krebs cycle enzymes, and the likely origin for this m+1 metabolite labeling is carboxylation of $^{13}CO_2$ catalyzed by pyruvate carboxylase to produce m+1 oxaloacetate. That this carboxylation resulted in equivalent labeling of malate and citrate compared with m+2 labeling from acetyl-CoA suggests that carboxylation in the retina and eyecup can keep pace with canonical carbon entry into the Krebs cycle and may in fact be a prevalent reaction.

Succinate oxidation and downstream Krebs cycle activity are rapid in eyecups (**Figure 2**),. That is surprising because succinate-dependent electron flux through complexes III and IV increase Δρ, and a high Δρ limits mitochondrial substrate oxidation. Oligomycin further simulates this feedback by blocking mitochondrial matrix proton influx through ATP synthase, causing Δρ to build to the point

where NADH oxidation by complex I and O_2 reduction by complex IV are not thermodynamically favorable. Respiration in the presence of oligomycin requires H^+ leak to partially relieve the block on respiratory chain activity. Our experiments show that oligomycin blocks glucose-stimulated respiration in eyecup tissue, and succinate overcomes the block, suggesting that it may dissipate Δρ or decrease the resistance of the mitochondrial membrane to H^+. NADH-linked substrates pyruvate and malate cannot mimic this large increase in mitochondrial respiration, suggesting that H^+ leak is unique to the biochemistry of succinate (**Figure 5A-B**). We titrated succinate in the presence of oligomycin and found that even low concentrations of extracellular succinate (<100 uM) can fuel leak respiration in the presence of oligomycin (also known as mitochondrial uncoupling).

We investigated the mechanism of succinate-induced uncoupling. Antioxidants, cyclosporine A, and carboxyatractyloside did not block oligomycin resistant OCR in eyecup tissue. Succinate-stimulated OCR is independent of oxidative stress-stimulated uncoupling protein activity, adenine nucleotide translocator (ANT) activity, and mitochondrial permeability transition pore complex activity (**Figure 5E-G**). Only rotenone inhibits succinate-stimulated, oligomycin-resistant OCR (**Figure 5H**). However, we found this effect simply reflects the loss of reducing power from glucose-derived NADH (**Figure 5I**). Together these data suggest that oligomycin stops complex I-driven OCR, yet this OCR resumes in the presence of succinate.

These results still do not explain the apparent H^+ leak in eyecup mitochondria; they only confirm that succinate consistently stimulates OCR in the presence of oligomycin. While we focus on eyecup tissue in this study, previous reports have demonstrated an exponential relationship between Δρ and H^+ leak in isolated mitochondria, particularly when the mitochondrial membrane is hyperpolarized (Brown & Brand, 1986; Nicholls, 1974). Increasing succinate flux in this system increases the polarity of the mitochondrial membrane, and consequently, H^+ leak. This H^+ leak was suggested to result from Δρ-dependent dielectric breakdown of the mitochondrial membrane (Nicholls, 1974). This mechanism of action for succinate is difficult to test conclusively in tissue. Follow-up investigations of our findings should focus on understanding the molecular and biophysical mechanism of succinate-induced uncoupling.

While succinate-induced mitochondrial uncoupling is possible in intact tissue *ex vivo* (**Figure 5**) or *in vitro* (Mills et al., 2018), we have yet to conclusively show that it occurs *in vivo*. The concentration of circulating succinate reaches up to 150 μM with obesity and 200 μM with type-2-diabetes (Serena et al., 2018), 150 μM during exercise in humans (Hochachka & Dressendorfer, 1976), and in excess of 300 μM when seals are forced to dive and become hypoxic (Hochachka et al., 1975). Most tissues are therefore not normally exposed to the millimolar [succinate] that elicit the most substantial effects on OCR, yet even lower [succinate] are able to stimulate oligomycin-resistant uncoupled respiration. The volume of subretinal space between RPE and photoreceptors is small [cite]. Succinate release from the retina (Bisbach et al., 2020), may populate the subretinal space with a [succinate] sufficient to stimulate mitochondrial uncoupling in eyecup tissue under physiological conditions. To determine if this occurs *in vivo* we will need to develop methods that can measure succinate concentrations within the tightly confined subretinal space.

Acknowledgements

- DH: T32 EY007031/EY/NEI NIH HHS/United States
- CB: F31 EY031165/EY/NEI NIH HHS/United States
- JBH: R01 EY006641/EY/NEI NIH HHS/United States
- JBH: R01 EY017863/EY/NEI NIH HHS/United States
- P30 DK017047/DK/NIDDK NIH HHS/United States (OCR studie and conscious jugular infusion studies were performed at the Cell Function Analysis Core of the Univ. of Washington's Diabetes Research Center, which is supported by NIH grant no….)

Author Contributions

DTH, CB, and JH conceived of the project, which was supervised by JBH. DTH, BMR, CB, EG, and TM performed the experiments. BMR, EG, TM, MS, and IRS provided critical methodological support. DTH and BMR analyzed the experiments. JBH and IRS provided reagents. DTH, CB, and JBH secured the funding. DTH wrote the original draft of the manuscript, which was reviewed and edited by all authors.

Declaration Of Interests

The authors declare no competing interests.

References

Andrienko, T. N., Pasdois, P., Pereira, G. C., Ovens, M. J., & Halestrap, A. P. (2017). The role of succinate and ROS in reperfusion injury - A critical appraisal. *J Mol Cell Cardiol*, *110*, 1-14. https://doi.org/10.1016/j.yjmcc.2017.06.016

Ayala J. E., Bracy D. P., Malabanan C., Freyja D. James F. D., Ansari T., Fueger P. T., McGuinness O. P., Wasserman D. H. (2011) Hyperinsulnemic-euglycemic clamps in conscious, unrestrained mice, *J Vis Exp*, (57): 3188, doi:10.3791/3188

Bertholet, A. M., Chouchani, E. T., Kazak, L., Angelin, A., Fedorenko, A., Long, J. Z., Vidoni, S., Garrity, R., Cho, J., Terada, N., Wallace, D. C., Spiegelman, B. M., & Kirichok, Y. (2019). H. *Nature*, *571*(7766), 515-520. https://doi.org/10.1038/s41586-019-1400-3

Bisbach, C. M., Hass, D. T., Robbings, B. M., Rountree, A. M., Sadilek, M., Sweet, I. R., & Hurley, J. B. (2020). Succinate Can Shuttle Reducing Power from the Hypoxic Retina to the O2 Rich Pigment Epithelium. *Cell Rep*, *31*(5), 107606. https://doi.org/10.1016/j.celrep.2020.107606

Brown, G. C., & Brand, M. D. (1986). Changes in permeability to protons and other cations at high proton motive force in rat liver mitochondria. *Biochem J*, *234*(1), 75-81. https://doi.org/10.1042/bj2340075

Du, J., Linton, J. D., & Hurley, J. B. (2015). Probing Metabolism in the Intact Retina Using Stable Isotope Tracers. *Methods Enzymol*, *561*, 149-170. https://doi.org/10.1016/bs.mie.2015.04.002

Ehinger, J. K., Piel, S., Ford, R., Karlsson, M., Sjövall, F., Frostner, E., Morota, S., Taylor, R. W., Turnbull, D. M., Cornell, C., Moss, S. J., Metzsch, C., Hansson, M. J., Fliri, H., & Elmér, E. (2016). Cell-permeable succinate prodrugs bypass mitochondrial complex I deficiency. *Nat Commun*, *7*, 12317. https://doi.org/10.1038/ncomms12317

Furchgott, R. F., & Shorr, E. (1948). The effect of succinate on respiration and certain metabolic processes of mammalian tissues at low oxygen tensions in vitro. *J Biol Chem*, *175*(1), 201-215.

Geubelle, P., Gilissen, J., Dilly, S., Poma, L., Dupuis, N., Laschet, C., Abboud, D., Inoue, A., Jouret, F., Pirotte, B., & Hanson, J. (2017). Identification and pharmacological characterization of succinate receptor agonists. *Br J Pharmacol*, *174*(9), 796-808. https://doi.org/10.1111/bph.13738

Gutiérrez-Aguilar, M., & Baines, C. P. (2013). Physiological and pathological roles of mitochondrial SLC25 carriers. *Biochem J*, *454*(3), 371-386. https://doi.org/10.1042/BJ20121753

Hanu, R., McKenna, M., O'Neill, A., Resneck, W. G., & Bloch, R. J. (2000). Monocarboxylic acid transporters, MCT1 and MCT2, in cortical astrocytes in vitro and in vivo. *Am J Physiol Cell Physiol*, *278*(5), C921-930. https://doi.org/10.1152/ajpcell.2000.278.5.C921

Hochachka, P. W., & Dressendorfer, R. H. (1976). Succinate accumulation in man during exercise. *Eur J Appl Physiol Occup Physiol*, *35*(4), 235-242. https://doi.org/10.1007/BF00423282

Hochachka, P. W., Owen, T. G., Allen, J. F., & Whittow, G. C. (1975). Multiple end products of anaerobiosis in diving vertebrates. *Comp Biochem Physiol B*, *50*(1), 17-22. https://doi.org/10.1016/0305-0491(75)90292-8

Jang, C., Hui, S., Zeng, X., Cowan, A. J., Wang, L., Chen, L., Morscher, R. J., Reyes, J., Frezza, C., Hwang, H. Y., Imai, A., Saito, Y., Okamoto, K., Vaspoli, C., Kasprenski, L., Zsido, G. A., Gorman, J. H.,

Gorman, R. C., & Rabinowitz, J. D. (2019). Metabolite Exchange between Mammalian Organs Quantified in Pigs. *Cell Metab*, *30*(3), 594-606.e593. https://doi.org/10.1016/j.cmet.2019.06.002

Kaufhold, M., Schulz, K., Breljak, D., Gupta, S., Henjakovic, M., Krick, W., Hagos, Y., Sabolic, I., Burckhardt, B. C., & Burckhardt, G. (2011). Differential interaction of dicarboxylates with human sodium-dicarboxylate cotransporter 3 and organic anion transporters 1 and 3. *Am J Physiol Renal Physiol*, *301*(5), F1026-1034. https://doi.org/10.1152/ajprenal.00169.2011

MacDonald, M. J., Fahien, L. A., Mertz, R. J., & Rana, R. S. (1989). Effect of esters of succinic acid and other citric acid cycle intermediates on insulin release and inositol phosphate formation by pancreatic islets. *Arch Biochem Biophys*, *269*(2), 400-406. https://doi.org/10.1016/0003-9861(89)90123-9

Millard, P., Delépine, B., Guionnet, M., Heuillet, M., Bellvert, F., & Létisse, F. (2019). IsoCor: isotope correction for high-resolution MS labeling experiments. *Bioinformatics*, *35*(21), 4484-4487. https://doi.org/10.1093/bioinformatics/btz209

Mills, E. L., Pierce, K. A., Jedrychowski, M. P., Garrity, R., Winther, S., Vidoni, S., Yoneshiro, T., Spinelli, J. B., Lu, G. Z., Kazak, L., Banks, A. S., Haigis, M. C., Kajimura, S., Murphy, M. P., Gygi, S. P., Clish, C. B., & Chouchani, E. T. (2018). Accumulation of succinate controls activation of adipose tissue thermogenesis. *Nature*, *560*(7716), 102-106. https://doi.org/10.1038/s41586-018-0353-2

Nakai, M., Chen, L., & Nowak, R. A. (2006). Tissue distribution of basigin and monocarboxylate transporter 1 in the adult male mouse: a study using the wild-type and basigin gene knockout mice. *Anat Rec A Discov Mol Cell Evol Biol*, *288*(5), 527-535. https://doi.org/10.1002/ar.a.20320

Neal A., Roundtree, A. M., Philips, C. W. Kavanagh, T. J., Williams D. P., Newham, P., Khalil G., Cook, D. L., Sweet, I. R. (2015). Quantification of Low-Level Drug Effects Using Real-Time, *in vitro* Measurement of Oxygen Consumption Rate. *Toxicol Sci*, 148(2), 594-602. https://doi.org/10.1093/toxsci/kfv208

Nicholls, D. G. (1974). The influence of respiration and ATP hydrolysis on the proton-electrochemical gradient across the inner membrane of rat-liver mitochondria as determined by ion distribution. *Eur J Biochem*, *50*(1), 305-315. https://doi.org/10.1111/j.1432-1033.1974.tb03899.x

Pajor, A. M. (2014). Sodium-coupled dicarboxylate and citrate transporters from the SLC13 family. *Pflugers Arch*, *466*(1), 119-130. https://doi.org/10.1007/s00424-013-1369-y

Parilla, J. H., Willard, J. R., Barrow, B. M., & Zraika, S. (2018). A Mouse Model of Beta-Cell Dysfunction as Seen in Human Type 2 Diabetes. *J Diabetes Res*, *2018*, 6106051. https://doi.org/10.1155/2018/6106051

Prag, H. A., Gruszczyk, A. V., Huang, M. M., Beach, T. E., Young, T., Tronci, L., Nikitopoulou, E., Mulvey, J. F., Ascione, R., Hadjihambi, A., Shattock, M. J., Pellerin, L., Saeb-Parsy, K., Frezza, C., James, A. M., Krieg, T., Murphy, M. P., & Aksentijević, D. (2020). Mechanism of succinate efflux upon reperfusion of the ischemic heart. *Cardiovasc Res*. https://doi.org/10.1093/cvr/cvaa148

Reddy, A., Bozi, L. H. M., Yaghi, O. K., Mills, E. L., Xiao, H., Nicholson, H. E., Paschini, M., Paulo, J. A., Garrity, R., Laznik-Bogoslavski, D., Ferreira, J. C. B., Carl, C. S., Sjøberg, K. A., Wojtaszewski, J. F. P., Jeppesen, J. F., Kiens, B., Gygi, S. P., Richter, E. A., Mathis, D., & Chouchani, E. T. (2020). pH-Gated Succinate Secretion Regulates Muscle Remodeling in Response to Exercise. *Cell*, *183*(1), 62-75.e17. https://doi.org/10.1016/j.cell.2020.08.039

Robb, E. L., Hall, A. R., Prime, T. A., Eaton, S., Szibor, M., Viscomi, C., James, A. M., & Murphy, M. P. (2018). Control of mitochondrial superoxide production by reverse electron transport at complex I. *J Biol Chem*, *293*(25), 9869-9879. https://doi.org/10.1074/jbc.RA118.003647

Serena, C., Ceperuelo-Mallafré, V., Keiran, N., Queipo-Ortuño, M. I., Bernal, R., Gomez-Huelgas, R., Urpi-Sarda, M., Sabater, M., Pérez-Brocal, V., Andrés-Lacueva, C., Moya, A., Tinahones, F. J., Fernández-Real, J. M., Vendrell, J., & Fernández-Veledo, S. (2018). Elevated circulating levels of succinate in human obesity are linked to specific gut microbiota. *ISME J*, *12*(7), 1642-1657. https://doi.org/10.1038/s41396-018-0068-2

Sweet, I. R., Cook, D. L., Wiseman, R. W., Greenbaum, C. J., Lernmark, A., Matsumoto, S., Teague, J. C., & Krohn, K. A. (2002). Dynamic perifusion to maintain and assess isolated pancreatic islets. *Diabetes Technol Ther*, *4*(1), 67-76. https://doi.org/10.1089/15209150252924111

Walters J. M., Ward G. M., Kalfas A., Best J. D., Alford F. P. (2016) The effect of epinephrine on glucose-mediated and insulin-mediated glucose disposal in insulin-dependent diabetes. *Metabolism*, 41(6); 671-677. doi: 10.1016/0026-0495(92)90062F

Wang, T., Xu, Y. Q., Yuan, Y. X., Xu, P. W., Zhang, C., Li, F., Wang, L. N., Yin, C., Zhang, L., Cai, X. C., Zhu, C. J., Xu, J. R., Liang, B. Q., Schaul, S., Xie, P. P., Yue, D., Liao, Z. R., Yu, L. L., Luo, L., Zhou, G.,

Yang, J. P., He, Z. H., Du, M., Zhou, Y. P., Deng, B. C., Wang, S. B., Gao, P., Zhu, X. T., Xi, Q. Y., Zhang, Y. L., Shu, G., & Jiang, Q. Y. (2020). Succinate induces skeletal muscle fiber remodeling via SUCNR1 signaling. *EMBO Rep*, *21*(5), e50461. https://doi.org/10.15252/embr.202050461

Windeløv J. A., Pedersen J., Holst **J. J.** (2016) Use of anesthesia dramatically alters the oral glucose tolerance and insulin secretion in C57Bl/6 mice. Physiol Rep. 4(11):e12824. doi: 10.14814/phy2.12824.

Figure Captions

Figure 1. Extracellular Succinate Increases Oxygen Consumption in Diverse Tissues Ex Vivo. (**A**) Schematic of the mitochondrial electron transport chain, the main site of O_2 consumption in the mammalian cell. We measured O_2 consumption rate (OCR) in freshly dissected (**C**) liver (n=3), (**D**) kidney (n=4), (**E**) interscapular brown adipose (n=3)), (**F**) cerebellum (n=3), (**B,G**) eyecup (n=3), and (**B,H**) retina (n=4) tissue from C57BL6/J mice, perifused in modified KRB buffer with 5 mM glucose as the principal metabolic fuel. We supplied this media with increasing concentrations of sodium succinate (30 μM, 100 μM, 300 μM, 1 mM, 3 mM, 10 mM, 30 mM, or 100 mM) and determined the consequent OCR. Example data from such experiments are shown in (B), with each line representing an individual sample. These data are summarized for different tissues in C-H as dots displaying mean steady-state OCR ± SEM. We estimated the dependence of OCR on [succinate] by fitting the data with an allosteric sigmoidal curve (red lines). Best-fit parameters are available in table 1. Dotted lines surrounding the curves represent 95% confidence intervals from the curve fit.

Figure 2. Systemic Metabolism of Infused Succinate
(**A-B**) We infused U-^{13}C-succinate into the mouse bloodstream and sampled blood 0.5 (n=5), 1 (n=5), 2 (n=7), 3 (n=6), 4 (n=5), 5 (n=7), 7.5 (n=6), and 10 (n=6) minutes post-infusion, with catheterized, un-infused mice as a “0 minute” control (n=7). **(A)** We measured unlabeled (m+0) and fully ^{13}C-labeled (m+4) succinate in blood post-infusion (plotted: mean ± SEM) and fit these data with a one-phase decay function (fit line ± 95% CI) **(B)** Isotopic abundance of blood succinate prior to (blue) and following (purple) infusion. Represented are individual replicates (dots) and mean ± SEM (bars). (**C-E**) Five minutes following the infusion, blood succinate enters in to and is metabolized by retina (n=3), cerebellum (n=3), eyecup (n=3), liver (n=4), lung (n=3), BAT (n=3), WAT (n=3), and blood (n=7). (**C**) m+4 succinate concentration within tissues shows differential tissue entry. (**D**) Fractional labeling of m+4 succinate shows relative replacement of the succinate pool by labeled substrate five minutes following the infusion, and (**E**) ^{13}C/^{12}C is a ratio that in each tissue represents relative extents to which the metabolites we measure (any of which could be a product of ^{13}C-succinate; table 2) are labeled by ^{13}C, relative to total ^{13}C abundance in that tissue. (**F**) Contains a representation of succinate’s position in the Krebs cycle and which carbons should be labeled (purple filled circles) by metabolism of infused U-^{13}C succinate, as opposed to unlabeled carbons (purple-rimmed unfilled circles). The abundance of ^{13}C-labeled metabolites downstream of succinate (m+4 fumarate (**G**), m+4 malate (**H**), m+4 citrate (**I**), m+4 aspartate (**J**), and m+3 pyruvate (**K**)) relative to tissue m+4 succinate is respectively represented. Individual data points are represented in panels C-K, with a red horizontal line with error bars reporting the mean ± SEM.

Figure 3. Infused Succinate Reveals Diverse Metabolic Routes in the Retina and Eyecup
Following bloodstream infusion of U-^{13}C-succinate in retina and eyecup, we determined the fractional labeling (**A-B, D-E, G-H, M-N**) and total abundance (metabolite pool size; **C, F, I, L, O**) of succinate (**A-C)**, malate **(D-F)**, aspartate (**G-I**), citrate (**J-L**), and α-ketoglutarate (**M-O**) 1, 2, 3, 5, and 12 minutes post-infusion. We compared these to labeling of tissue from un-infused catheterized C57BL6/J mice (“0 minutes”). M+*x* indicates that the molecule is ^{13}C-labeled with *x* carbons, all originating from infused succinate. N=3 for all time points except 12 minutes post-infusion, where n=6. All bars and dots represent mean ± SEM.

Figure 4. Infused Succinate Is Utilized to Make Glycolytic Precursors in Retina and Eyecup Tissue. (A) We determined m+3 phosphoenolpyruvate / m+4 succinate in our tissue panel 5 minutes following infusion, displaying data as in Figure 2G-K, **(B)** Schematic of the metabolic route by which ^{13}C-succinate is most likely able to label glycolytic intermediates**. (C-K)** We performed the same analysis as in Figure 3 on pyruvate (**C-E**), phosphoenolpyruvate (PEP; **F-H**), and 3-phosphoglycerate (3-PG; **I-K**). N=3 for all time points except 12 minutes post-infusion, where n=6. All bars and dots represent mean ± SEM.

Figure 5. Extracellular Succinate Uncouples Eyecup Mitochondria *Ex Vivo*
(A) *Ex vivo* eyecup OCR as a function of substrate concentration in eyecups respiring using 5 mM glucose supplemented with increasing concentrations (30 µM, 100 µM, 300 µM, 1 mM, 3 mM, 10 mM) of succinate or equimolar malate and pyruvate. (**B**) We estimated mitochondrial H^+ flux from the matrix to the intermembrane space by multiplying OCR by the H^+/O_2 ratio [cite] for the pyruvate/malate-linked substrate NADH (10) or succinate (6). The disagreement in substrate-dependent H^+ flux between these curves suggests that additional H^+ flux in the succinate treatment is used to counter an additional H^+ conductance from the intermembrane space, suggesting that with succinate there is an H^+ conductance that is not from ATP-synthase activity. (**C**) We determined ATP-synthase-immune succinate or pyruvate/malate oxidation by incubating eyecup tissue first in 5 mM glucose, next in 5 mM glucose with 10 µM of the ATP-synthase inhibitor oligomycin A, and finally in a mix of 5 mM glucose, 10 µM oligomycin, and 5 mM of either succinate (black) or pyruvate/malate (blue). (**D**) Succinate exhibited substantial oligomycin-resistant respiration, and we determined how much respiration is oligomycin-immune as a function of [succinate], comparing this data to Figure 1G, converted to OCR per tissue unit rather than per unit mass. (**E-I**) To determine the source of this oligomycin-resistant respiration, we performed the experimental treatments described in (C), but following the addition of 5 mM succinate to increase respiration we attempted to shut down this increase by adding (**F**) the antioxidants mito-tempo (purple line) or N-acetyl cysteine (black line), the adenine nucleotide translocator inhibitor carboxyatractyloside (CATR), (**G**) the mitochondrial permeability transition pore complex inhibitor cyclosporine A (CsA), (**H**) the mitochondrial complex I inhibitor rotenone, (**I**) or by removing glucose then adding rotenone. Lines represent mean O_2 consumption rate following subtraction of the 5 mM glucose "baseline" (**A,B,D**) or the 3 mM KCN "floor" (**C,E-I**).

Table 1. Best-Fit Kinetic Parameters for *ex vivo* Succinate oxidation
Least squares fit, Parameters are represented as [mean (95% Confidence Interval)**]**

Tissue	V_{max} (nmol O_2 / mg / min)	$K_{1/2}$ ([succinate])	H*	R^2	n
Retina	0.35 (?**)	11.14 (0.4-?**)	0.4025 (0.14-1.2)	0.56	4
Cerebellum	0.36 (0.31-0.42)	2.72 (1.67-4.94)	1.38 (0.81-0.73)	0.90	3
Eyecup	0.41 (0.36-0.48)	2.22 (1.49-3.92)	1.10 (0.69-1.90)	0.95	3
Liver	0.89 (0.77-1.04)	0.90 (0.49-1.75)	1.40 (0.72-?**)	0.85	3
BAT	0.57 (0.51-0.66)	1.45 (0.9-2.58)	1.15 (0.72-2.04)	0.91	3
Kidney	0.66 (0.52-1.20)	1.50 (0.84-8.53)	1.21 (0.64-2.35)	0.88	4

** Hill's Slope*
*** "?" indicates that the curve fit is unable to estimate this parameter*

Table 2. Metabolites used to determine total ^{13}C labeling

Metabolic process	Metabolite Name	# carbons
Glycolysis	Dihydroxyacetone phosphate	3
Glycolysis	3-phosphoglycerate	3
Glycolysis	Phosphoenolpyruvate	3

Glycolysis	Pyruvate	3
Krebs Cycle	Citrate	6
Krebs Cycle	Isocitrate	6
Krebs Cycle	α-ketoglutarate	5
Krebs Cycle	fumarate	4
Krebs Cycle	malate	4
Krebs Cycle (anapleurotic)	aspartate	4
Krebs Cycle (anapleurotic)	glutamate	5

*****Although we routinely measure succinate, it was not included on this table because ^{13}C labeling on succinate could be indicative of residual infusate in the cytosol or blood-vessels.

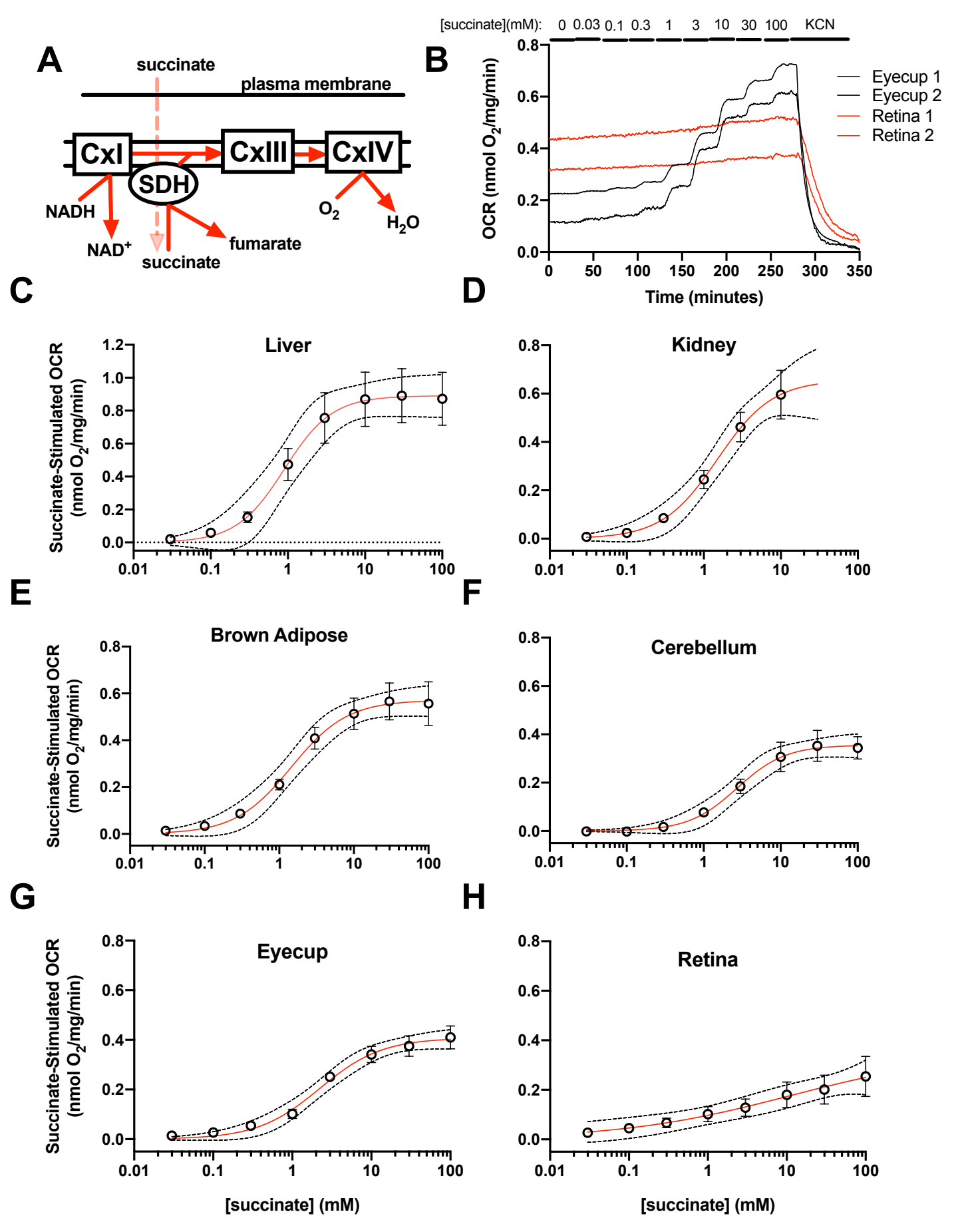
A
succinate
plasma membrane
CxI
CxIII
CxIV
SDH
NADH
NAD+
succinate
fumarate
O2
H2O
B
[succinate](mM): 0 0.03 0.1 0.3 1 3 10 30 100 KCN
OCR (nmol O2/mg/min)
Time (minutes)
Eyecup 1
Eyecup 2
Retina 1
Retina 2
C
Liver
D
Kidney
E
Brown Adipose
F
Cerebellum
G
Eyecup
H
Retina
Succinate-Stimulated OCR (nmol O2/mg/min)
[succinate] (mM)

Blood - Succinate

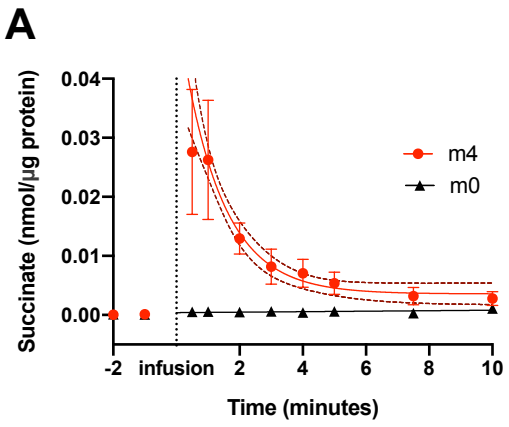

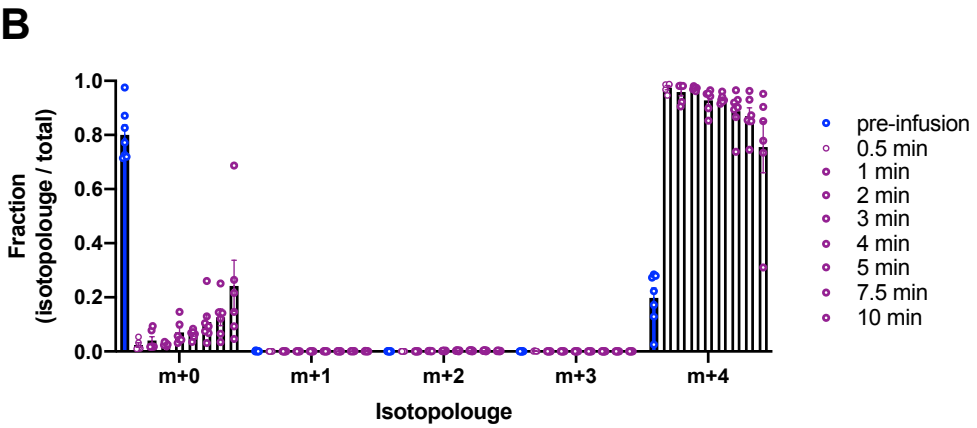

Tissue - Succinate Flux

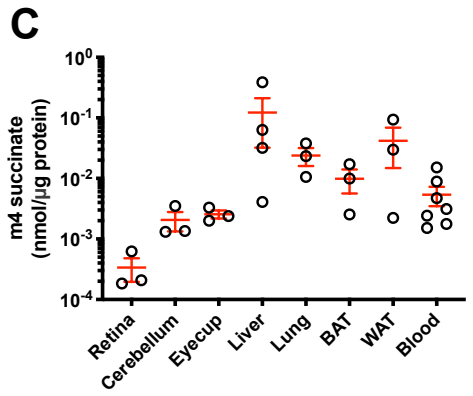

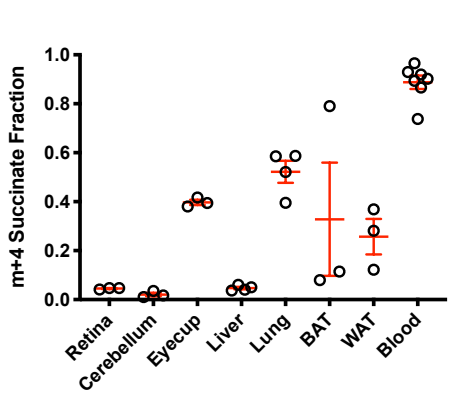

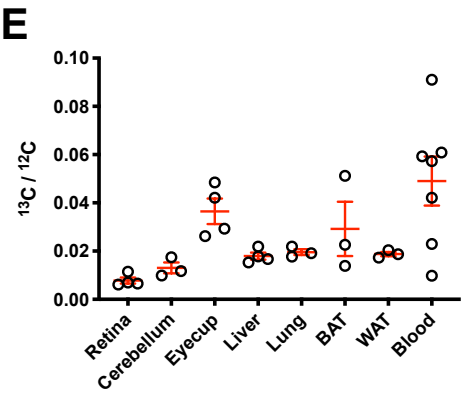

Tissue - Downstream Intermediates

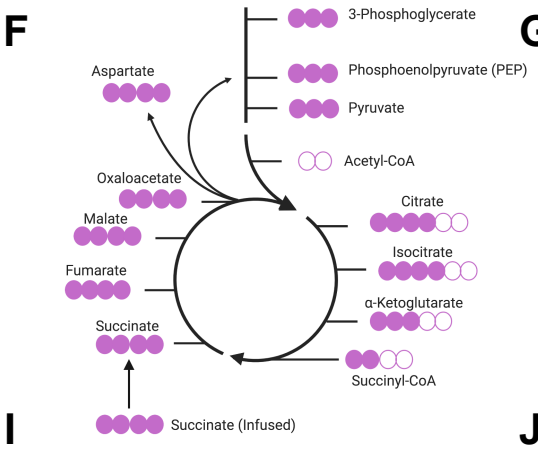

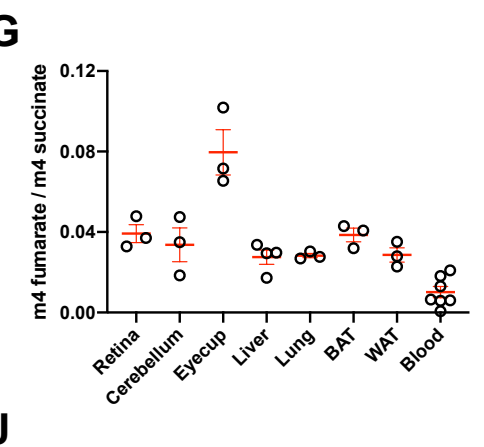

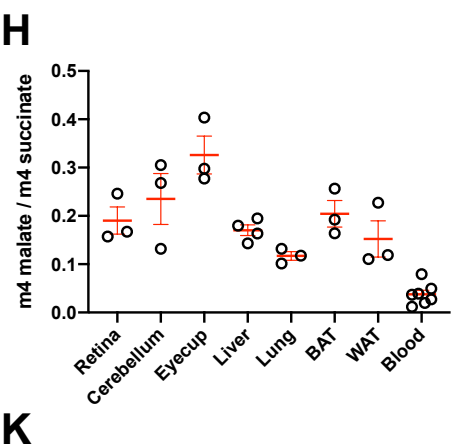

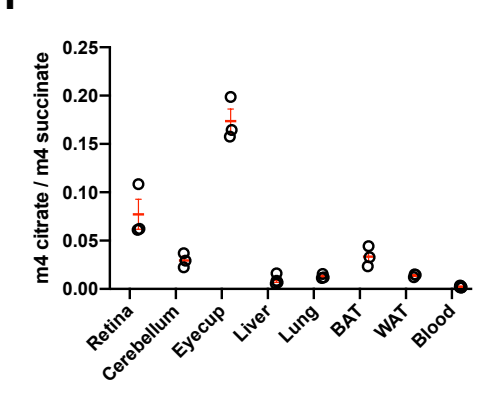

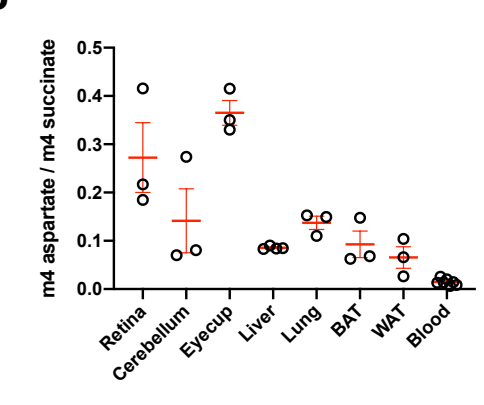

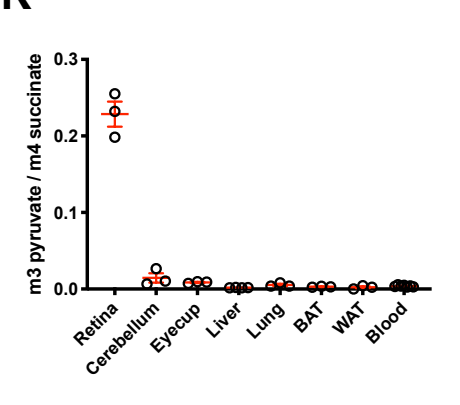

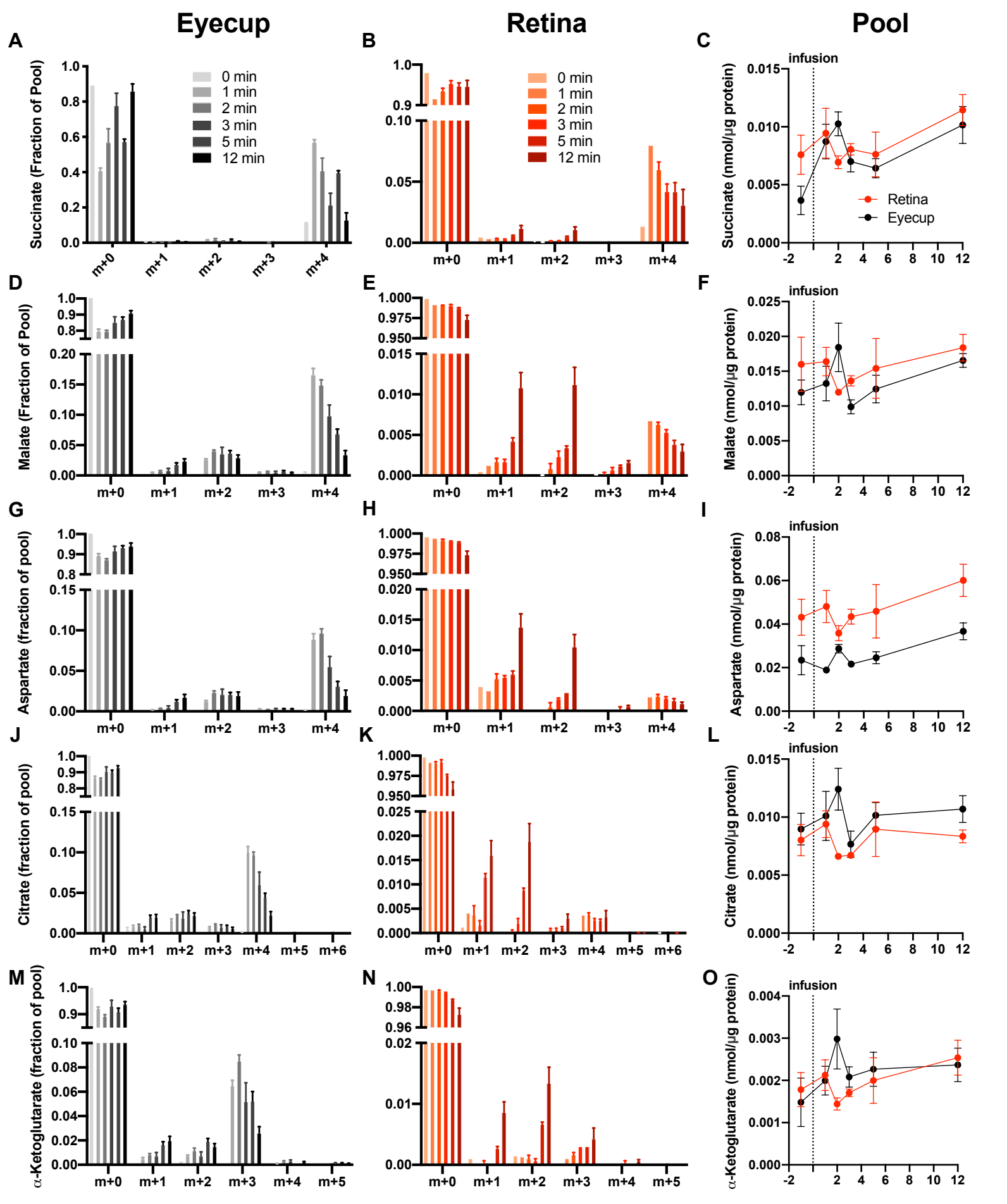
Eyecup
Retina
Pool
A
B
C
0 min
1 min
2 min
3 min
5 min
12 min
Succinate (Fraction of Pool)
Succinate (nmol/µg protein)
infusion
Retina
Eyecup
D
E
F
Malate (Fraction of Pool)
Malate (nmol/µg protein)
G
H
I
Aspartate (fraction of pool)
Aspartate (nmol/µg protein)
J
K
L
Citrate (fraction of pool)
Citrate (nmol/µg protein)
M
N
O
α-Ketoglutarate (fraction of pool)
α-Ketoglutarate (nmol/µg protein)
m+0
m+1
m+2
m+3
m+4
m+5
m+6

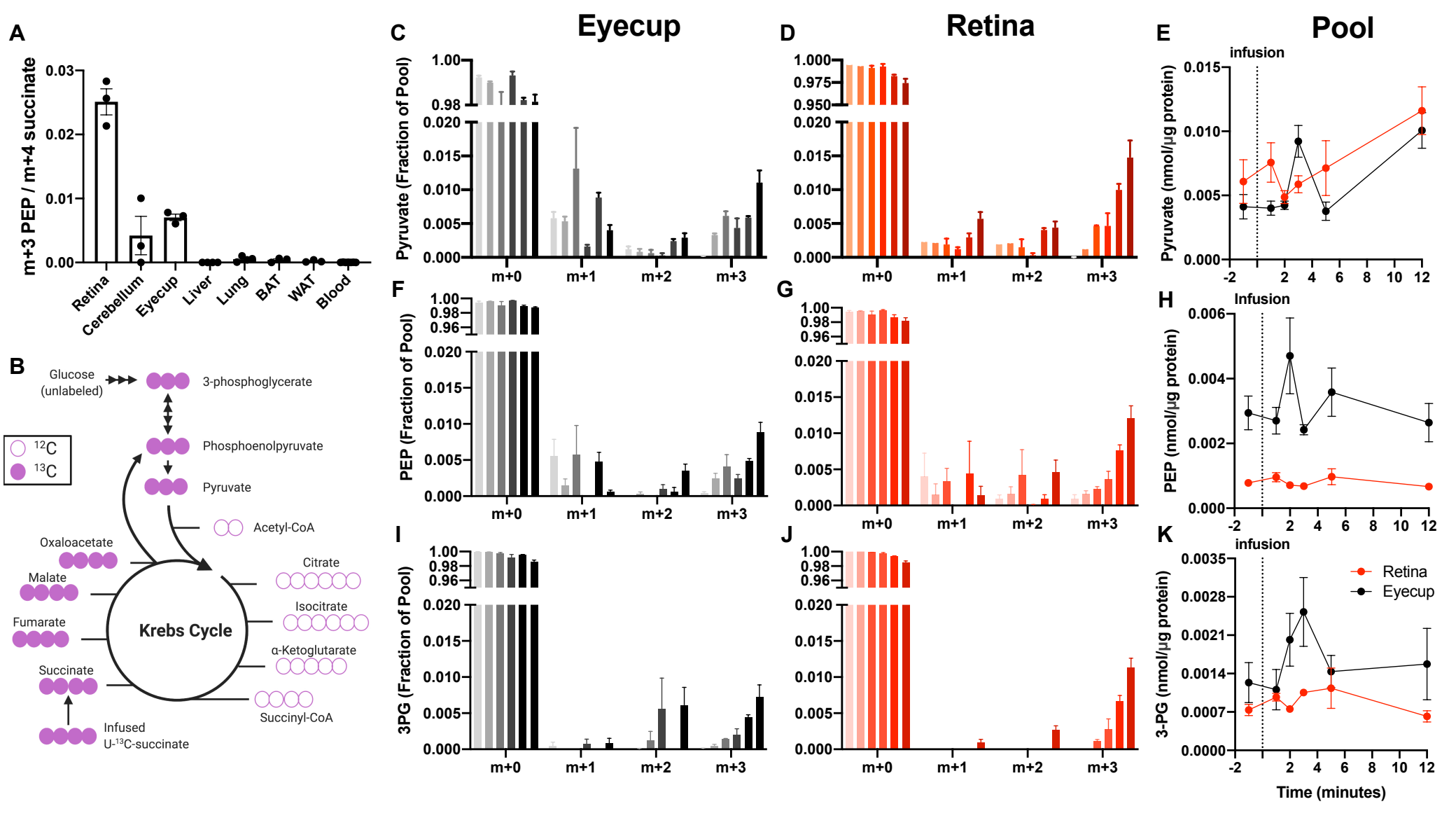
A
m+3 PEP / m+4 succinate
0.03
0.02
0.01
0.00
Retina
Cerebellum
Eyecup
Liver
Lung
BAT
WAT
Blood
B
Glucose (unlabeled)
3-phosphoglycerate
Phosphoenolpyruvate
Pyruvate
Acetyl-CoA
Citrate
Isocitrate
α-Ketoglutarate
Succinyl-CoA
Oxaloacetate
Malate
Fumarate
Succinate
Krebs Cycle
Infused U-13C-succinate
12C
13C
C
Eyecup
D
Retina
E
Pool
Pyruvate (Fraction of Pool)
PEP (Fraction of Pool)
3PG (Fraction of Pool)
m+0
m+1
m+2
m+3
F
G
I
J
infusion
Pyruvate (nmol/µg protein)
H
PEP (nmol/µg protein)
K
3-PG (nmol/µg protein)
Retina
Eyecup
Time (minutes)

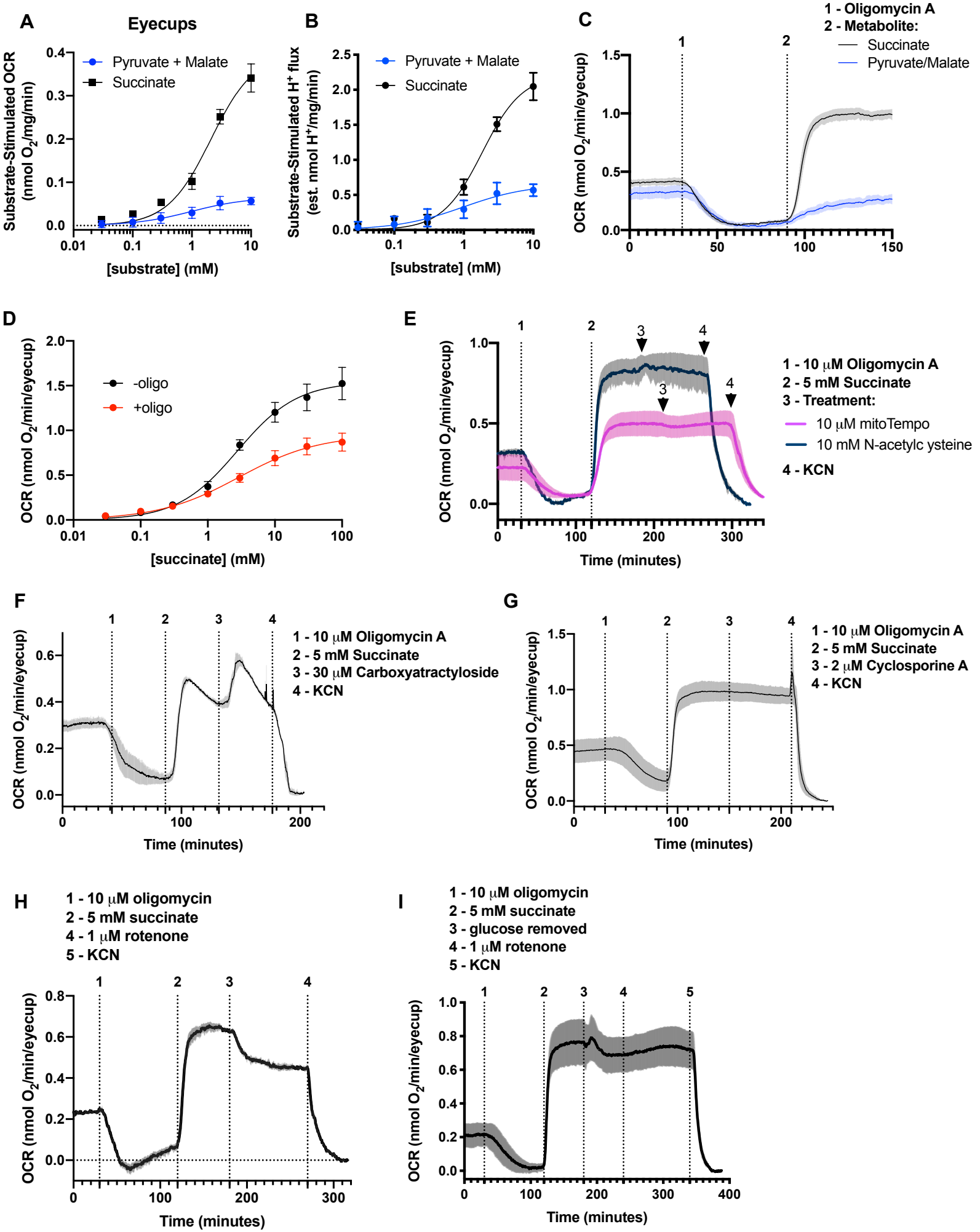
A
Eyecups
Pyruvate + Malate
Succinate
Substrate-Stimulated OCR (nmol O2/mg/min)
[substrate] (mM)
B
Pyruvate + Malate
Succinate
Substrate-Stimulated H+ flux (est. nmol H+/mg/min)
[substrate] (mM)
C
1 - Oligomycin A
2 - Metabolite:
Succinate
Pyruvate/Malate
OCR (nmol O2/min/eyecup)
D
-oligo
+oligo
OCR (nmol O2/min/eyecup)
[succinate] (mM)
E
1 - 10 μM Oligomycin A
2 - 5 mM Succinate
3 - Treatment:
10 μM mitoTempo
10 mM N-acetylc ysteine
4 - KCN
OCR (nmol O2/min/eyecup)
Time (minutes)
F
1 - 10 μM Oligomycin A
2 - 5 mM Succinate
3 - 30 μM Carboxyatractyloside
4 - KCN
OCR (nmol O2/min/eyecup)
Time (minutes)
G
1 - 10 μM Oligomycin A
2 - 5 mM Succinate
3 - 2 μM Cyclosporine A
4 - KCN
OCR (nmol O2/min/eyecup)
Time (minutes)
H
1 - 10 μM oligomycin
2 - 5 mM succinate
4 - 1 μM rotenone
5 - KCN
OCR (nmol O2/min/eyecup)
Time (minutes)
I
1 - 10 μM oligomycin
2 - 5 mM succinate
3 - glucose removed
4 - 1 μM rotenone
5 - KCN
OCR (nmol O2/min/eyecup)
Time (minutes)

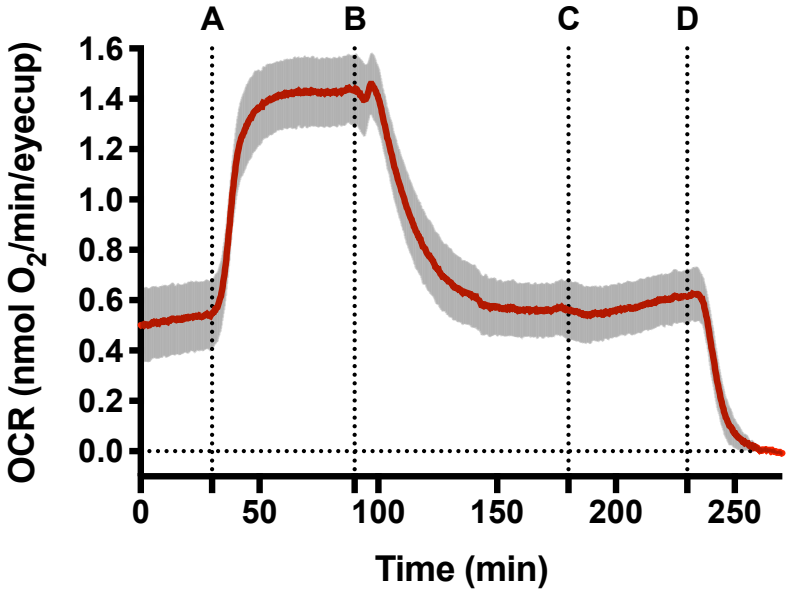

A: +5 mM succinate
B: -5 mM succinate
C: 500 μM *cis*-expoxysuccinate
D: KCN

Figure S1. SUCNR1 Agonism is insufficient to increase oxygen consumption. Eyecup tissue was dissected from C57BL6J mice and ex vivo oxygen consumption rate (OCR, mean±SEM) measured as described in the materials and methods section. At baseline (0-30 minutes) the only source of energy to eyecups to fuel OCR was 5 mM glucose. At time=30 (A) minutes 5 mM succinate was added, which increased OCR ~3-fold. Succinate was withdrawn (B) and OCR fell to control values. *Cis*-epoxysuccinate is a SUCNR1 agonist with 10x greater potency for the GPCR than succinate (Geubelle et al., 2017). (C) We added 500 μM cis-epoxysuccinate to the 5 mM glucose treatment to determine whether any increases in OCR were due to metabolic changes transduced by SUCNR1. (D) KCN was used to inhibit mitochondrial complex IV OCR activity to confirm that the OCR observed in this experiment was primarally mitochondrial. We did not find any immediate effects of SUCNR1 agonism on OCR that were comparable to those of succinate itself, suggesting that succinate-induced OCR occurs mainly through direct succinate oxidation and not downstream protein signaling. (n=4)

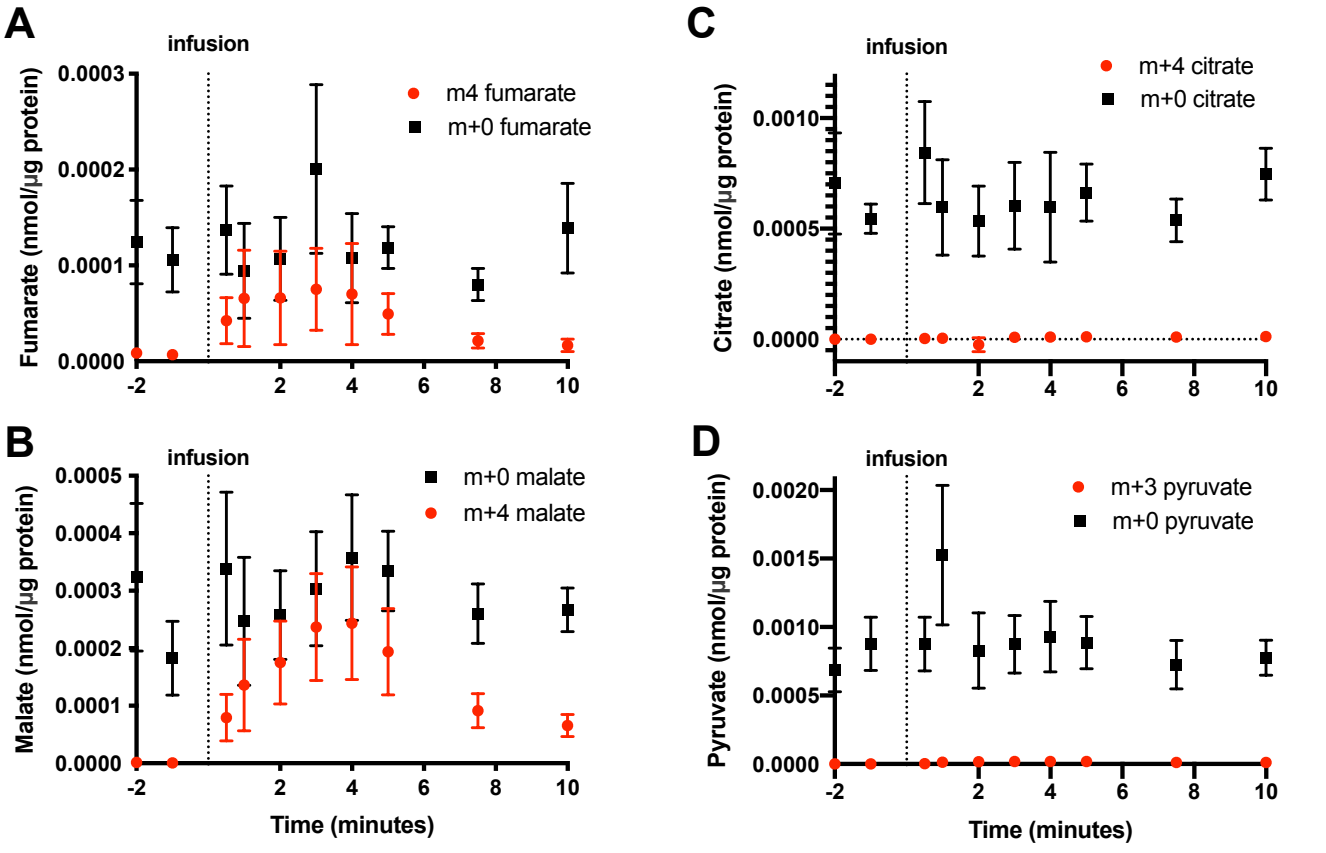

Figure S2. Post-Infusion blood Metabolite Labeling. U-^{13}C-succinate was infused into blood through a veinous catheter and 10 µL blood samples were drawn at 0.5, 1, 2, 3, 4, 5, 7.5, and 10 minutes post-infusion. Analysis of blood samples shows that following the infusion, succinate does turn over in whole blood to become (A) m+4 fumarate and (B) m+4 malate, while downstream (C) m+4 citrate and upstream (D) m+3 pyruvate appear relatively unperturbed, though this occurs to a far lesser extent than m+4 succinate turnover in blood, suggesting that rather than blood succinate feeding blood fumarate or malate pools, it is taken up into tissues. The formation of m+4 intermediates in blood does not appear to perturb the m+0 pools of unlabeled metabolic intermediates also in blood. (n=5-7)

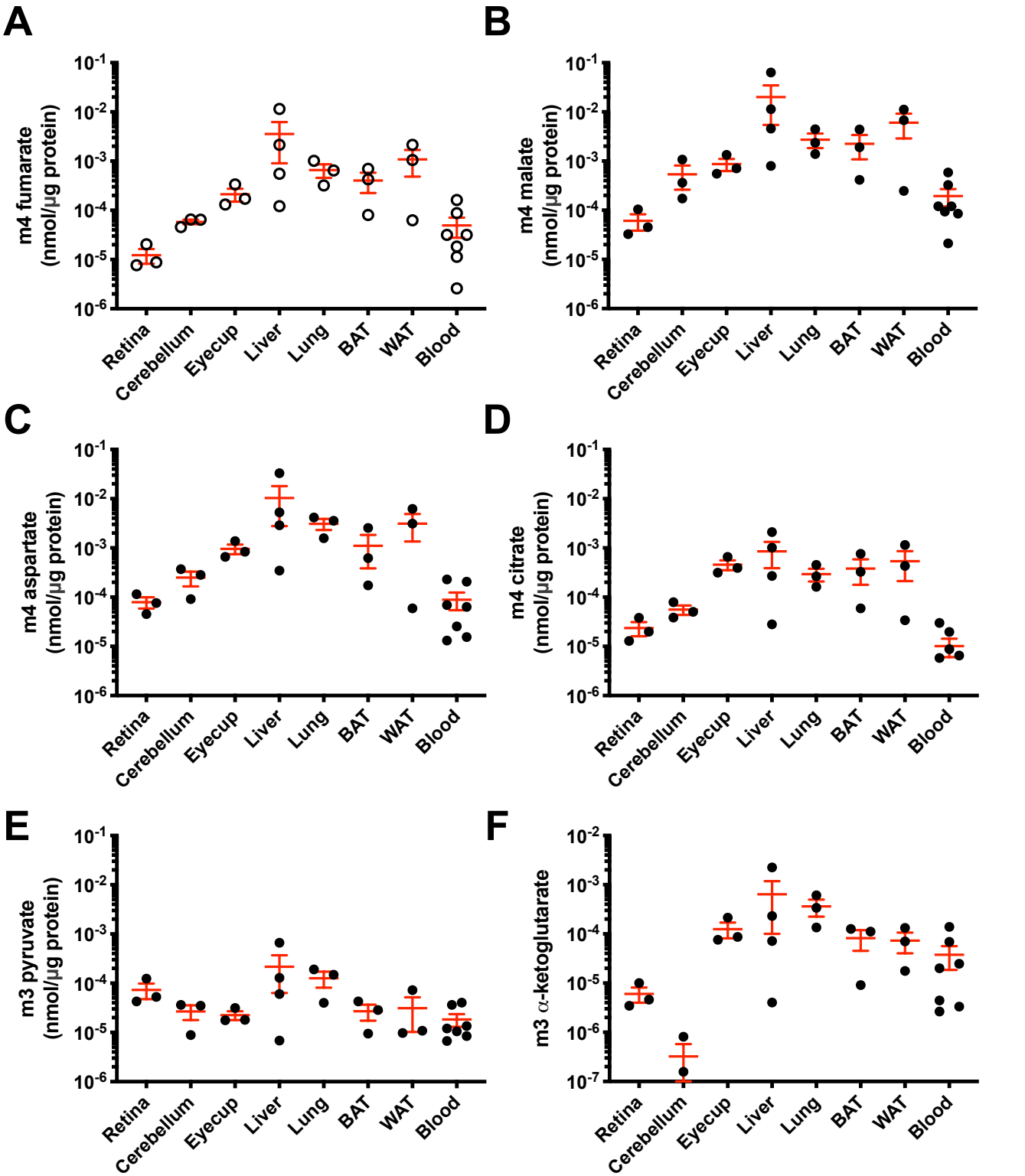

Figure S3. Abundance of labeled TCA cycle intermediates in various tissues 5 minutes following bloodstream succinate infusion. (A) m+4 fumarate, (B) m+4 malate, (C) m+4 aspartate, (D) m+4 citrate, (E) m+3 pyruvate, (F) and m+3 α–Ketoglutarate in retina, cerebellum, eyecup, liver, lung, BAT, WAT, and blood tissue. The labeling patterns of most downstream metabolic intermediates are subject to the amount of m+4 succinate imported into that tissue and thus the relative abundances of m+4 labeled matabolites closely matches that of m+4 succinate in tissues (n=3-4).

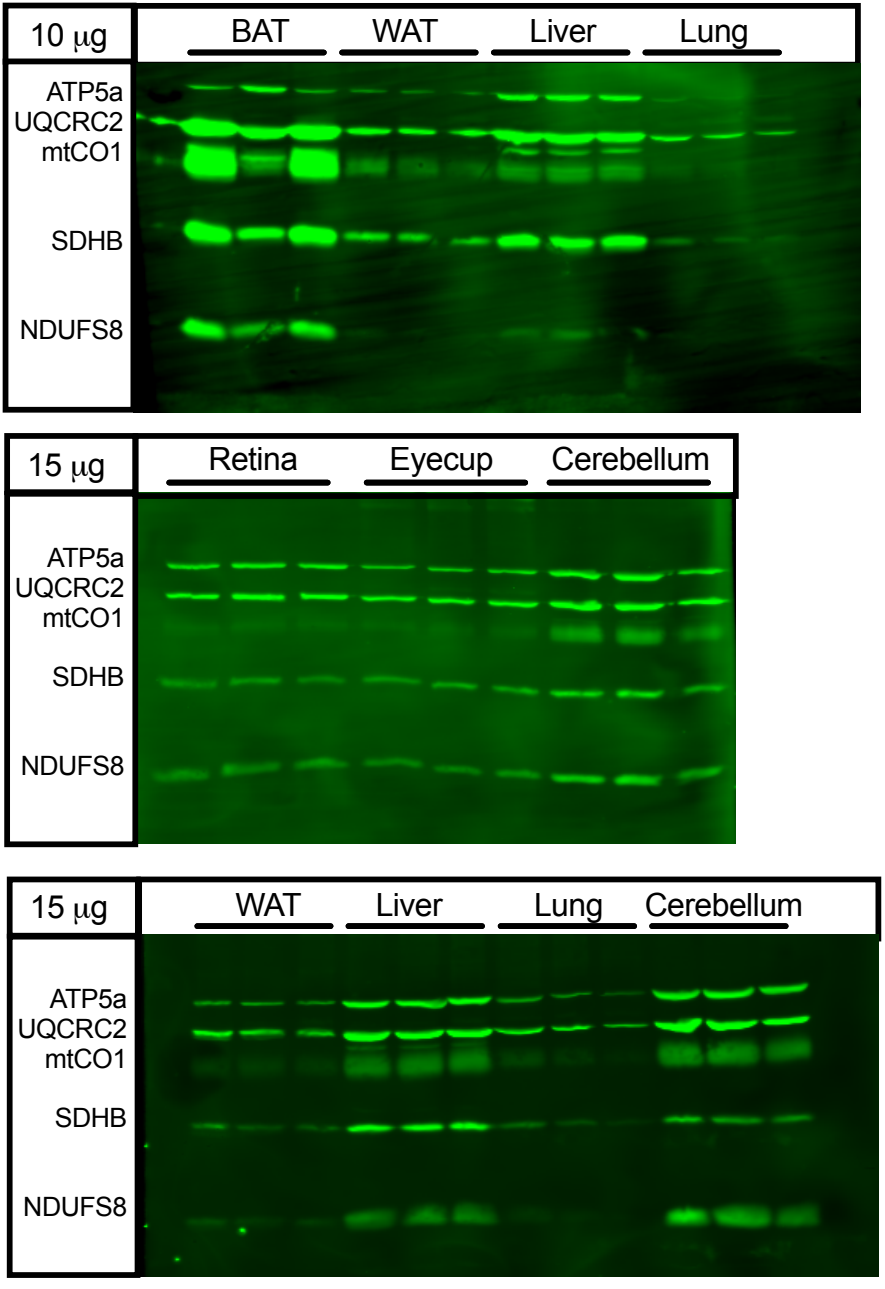

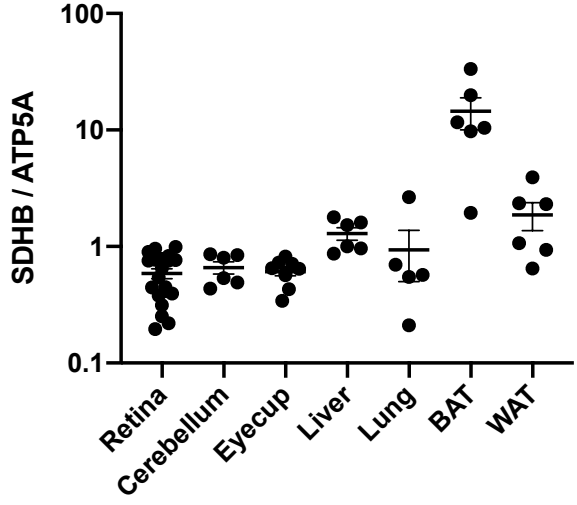

Figure S4. Mouse Succinate Dehydrogenase subunit B (SDHB) expression in a Panel of Tissues. Indicated tissues were dissected from young (~8 week old) C57BL6/J mice and lysed in RIPA buffer by sonication. Indicated protein amounts (top left corner of each blot) were loaded into and run on a 13% polyacrylamide gel, and transferred to a PVDF membrane prior to blocking and immunolabeling using a mouse anti-Total OXPHOS antibody (abcam, ab110413, diluted 1:1000). To determine mitochondrial SDHB levels, we normalized SDHB levels to those of the ATP synthase subunit ATP5a and plotted noramlized SDHB/ATP5a values for retina, cerebellum, eyecup, liver, lung, BAT, and WAT obtained across multiple blots. Mean±SEM, n=5-20, 1 outlying lung sample was excluded from this data.

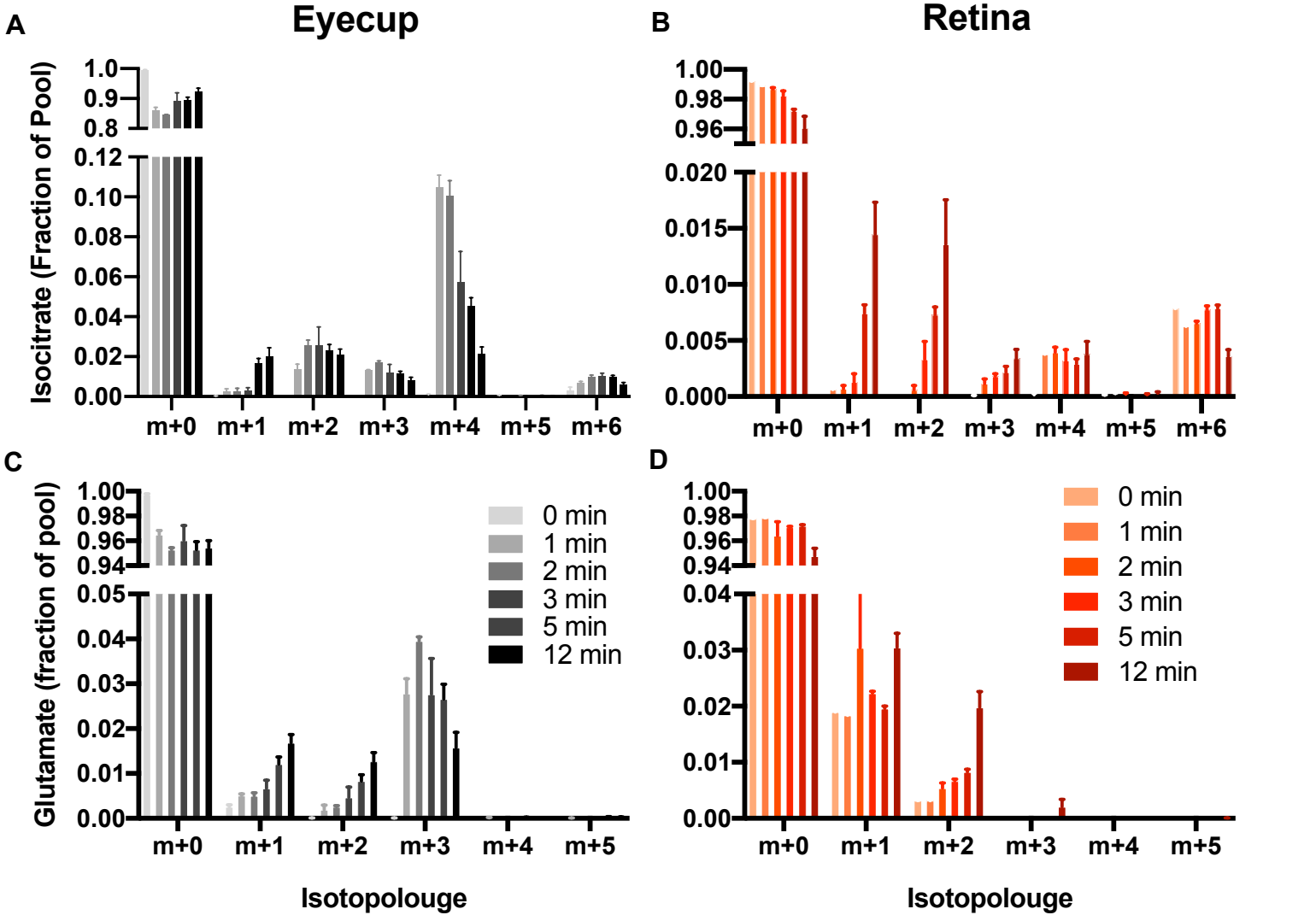

Figure S5. Isocitrate and Glutamate Isotopolouge Distributions in Retina and Eyecup Tissue Following *In Vivo* U-^{13}C-Succinate Infusion.

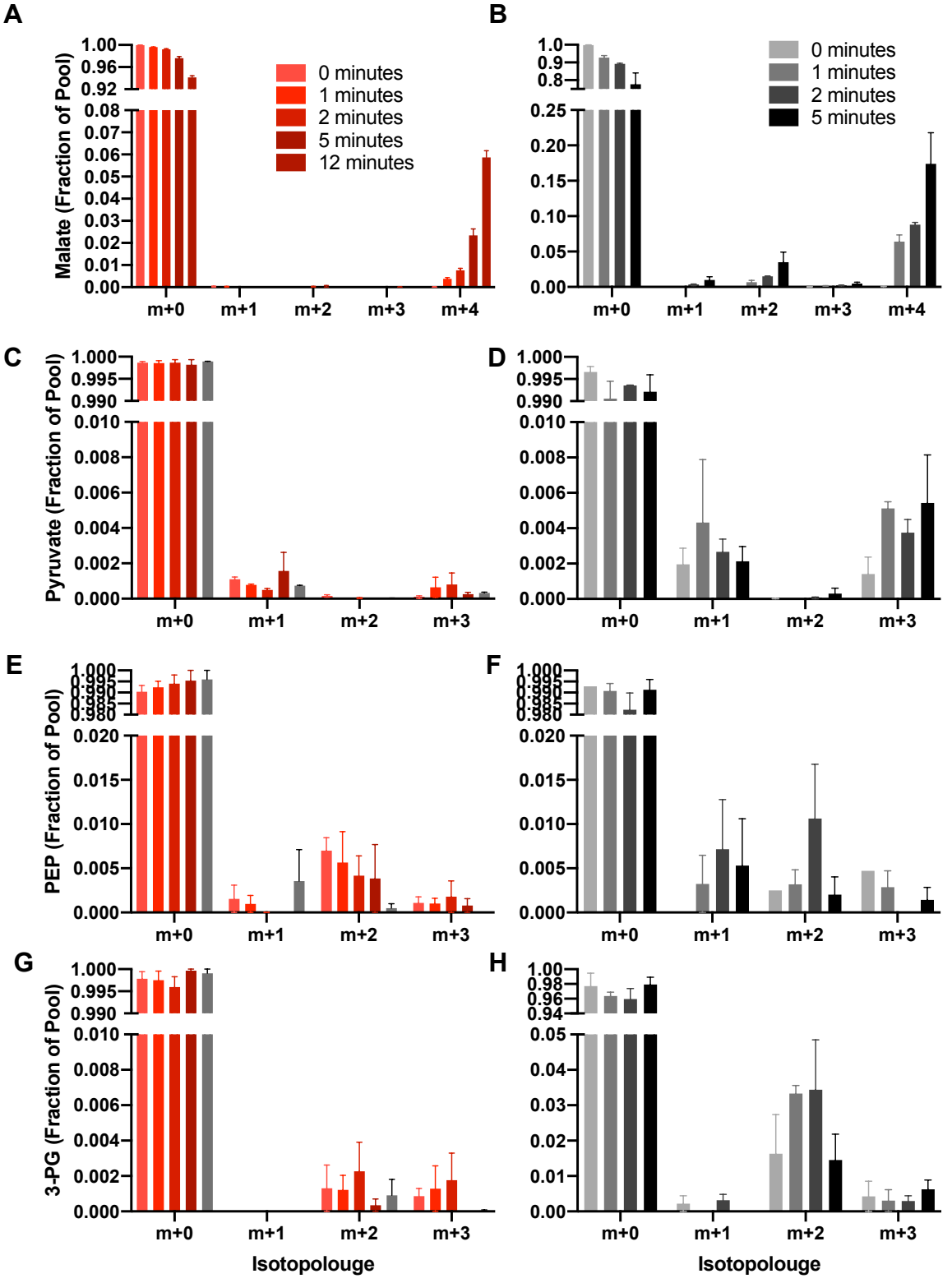

Figure S6. Lack of Gluconeogenesis in *Ex Vivo* Retina and Eyecup Tissue. Retina and Eyecup tissue was dissected from C57BL6/J mice in Hanks buffered salt solution. The tissue was next incubated in a Krebs-Ringer Bicarbonate Buffer supplemented with 5 mM glucose and 50 μM U-^{13}C-succinate equillibrated to 37°C at 5% CO_2 (n=1-3). Tissues were incubated in this buffer for 0, 1, 2, or 5 minutes and flash-frozen in liquid N_2. Tissue was homogenized, derivitized, and metabolite abundance determined using gas chromatography-mass spectrometry. Relative isotopolouge abundance was determined and is plotted for (A-B) malate, (C-D) pyruvate, (E-F) PEP, and (G-H) 3-PG. While carbons from labeled succinate do appear on Krebs cycle intermediates in both tissues (A-B) , they do not appear to accumulate m+3 labeling on Pyruvate, PEP, or 3-PG (C-H) linerarly over time as they do in vivo (Figure 4).